

Should I Stay or Should I Go: Stellar Wind Retention and Expulsion in Massive Star Clusters

J. P. Naiman¹*, E. Ramirez-Ruiz², D. N. C. Lin²

¹Harvard-Smithsonian Center for Astrophysics, 60 Garden Street, Cambridge, MA, 02138, USA

²Department of Astronomy and Astrophysics, University of California, Santa Cruz, CA 95064, USA

11 July 2017

ABSTRACT

Mass and energy injection throughout the lifetime of a star cluster contributes to the gas reservoir available for subsequent episodes of star formation and the feedback energy budget responsible for ejecting material from the cluster. In addition, mass processed in stellar interiors and ejected as winds has the potential to augment the abundance ratios of currently forming stars, or stars which form at a later time from a retained gas reservoir. Here we present hydrodynamical simulations that explore a wide range of cluster masses, compactnesses, metallicities and stellar population age combinations in order to determine the range of parameter space conducive to stellar wind retention or wind powered gas expulsion in star clusters. We discuss the effects of the stellar wind prescription on retention and expulsion effectiveness, using MESA stellar evolutionary models as a test bed for exploring how the amounts of wind retention/expulsion depend upon the amount of mixing between the winds from stars of different masses and ages. We conclude by summarizing some implications for gas retention and expulsion in a variety of compact ($\sigma_v \gtrsim 20 \text{ km s}^{-1}$) star clusters including young massive star clusters ($10^5 \lesssim M/M_\odot \lesssim 10^7$, $age \lesssim 500 \text{ Myrs}$), intermediate age clusters ($10^5 \lesssim M/M_\odot \lesssim 10^7$, $age \approx 1 - 4 \text{ Gyrs}$), and globular clusters ($10^5 \lesssim M/M_\odot \lesssim 10^7$, $age \gtrsim 10 \text{ Gyrs}$).

Key words: galaxies: star clusters: general – stars: mass-loss – (Galaxy:) globular clusters: general

1 INTRODUCTION

Whether and when gas is retained within a star cluster, along with inter-cluster and intra-cluster gas heating mechanisms determines the star formation history of the cluster. Many cluster properties can be responsible for gas retention or expulsion in a cluster - the cluster's compactness, cluster mass, ability to cool effectively, mass and temperature of gas reservoir, and efficiency of internal and external heating mechanisms. As it is thought that most stars form in clusters (e.g. Lada & Lada 2003), the study of which parameters and mechanisms are important at different cluster evolutionary times is crucial to understand when favorable conditions for star formation arise throughout a cluster's lifetime.

Observations of young massive clusters (YMCs), intermediate age clusters (IACs) and globular clusters (GCs) potentially give us insights into gas retention at different times within massive star clusters (e.g. Bastian & Lardo 2017). Additionally, if GCs evolve from YMCs and IACs as some have suggested (Longmore et al. 2014; Kruijssen 2015) then observations of each type of system provides clues to the origin of the high level of occurrence of multiple subpopulations with different abundance ratios within present day GCs.

Variations in the abundances of He, Mg, C, N, O, Mg, Na and Al in main sequence stars (Gratton et al. 2001; Briley et al. 2002; Cohen et al. 2002; Cannon et al. 1998; Pancino et al. 2010b) and RGB stars (Sneden et al. 2004) within the majority of Galactic globular clusters suggest a complex enrichment history during the formation of stars

within these systems. In addition, the observed anti-correlations between several elements (Na-O and Mg-Al; Kraft et al. 1993; Ivans et al. 1999; Carretta et al. 2006, 2009a; Conroy 2012) require a significant fraction of the enriching material to be processed at temperatures $> 10^7 \text{ K}$ in order for the CNO, Na-Ne and Mg-Al cycles to be activated (Karakas & Lattanzio 2007; Ventura & D'Antona 2008b). As the anomalous population is responsible for 30-70% of the stellar content of the globular clusters (e.g. Carretta et al. 2009b) any scenario invoked to explain this complex star formation history must also account for the pollution of a significant portion of the stellar population or the removal of the majority of the unpolluted first generation of stars. Additionally, the spatial distributions of anomalous stars, individual stellar abundance spreads, limits on the initial mass of globular clusters and various other constraints must be considered in any process capable of producing multiple episodes of star formation in YMCs if they are indeed the progenitors of current globular clusters (Bastian et al. 2013a; Kruijssen 2015).

Several mechanisms have been proposed to explain these abundance variations. While some rely directly on gas retention and protracted enrichment of populations of stars formed after the initial burst of star formation (Prantzos et al. 2007; Ventura & D'Antona 2008a,b; Pfleiderer-Altenburg & Kroupa 2009; D'Ercole et al. 2010; Conroy et al. 2011) others rely on enrichment processes which occur during one main star formation event (Bastian et al. 2013a; de Mink et al. 2009; Denissenkov & Hartwick 2014; Prantzos & Charbonnel 2006). Whether directly or indirectly, stellar winds can play an important role in the retention or expulsion of gas during enrichment processes - if hot stellar winds thermalize efficiently with other

* E-mail: jill.naiman@cfa.harvard.edu

sources of gas they can drive material out of a star cluster, while if cold stellar winds are added to the intercluster medium they can aid in the rapid cooling of the gas and help to trigger star formation. Thus, a careful study of gas retention and expulsion from stellar winds is a necessary component of understanding what cluster potential parameters and ages are favorable for gas retention, and what combinations lead to an overall expulsion of gas from the system.

In the context of wind retention in proto-globular clusters, there have been several one dimensional simulations of gas over a small range of wind and cluster parameters, particularly for slow AGB winds ($v_w = 10 \text{ km s}^{-1}$), in the presence of supernovae and star formation (e.g. D'Ercole et al. 2008). Additionally, a parametric study of the role of cluster mass and compactness has been done, albeit using only a limited range of structural parameters (Vesperini et al. 2010). There have also been several detailed three dimensional studies focused on stellar wind retention/expulsion in star clusters (GCs; Calura et al. 2015; Priestley et al. 2011, T Tauri/Herbig Ae/Be star clusters; Rodríguez-González et al. 2008, OB clusters; Rogers & Pittard 2013), however, to study the interaction of a wide range of stellar wind parameters from various stellar population ages along with a variety of stellar cluster masses and compactnesses the required full simulation suite over all parameter space in three dimensions would be computationally prohibitive.

Because of their shallow potentials, careful treatment of stellar winds within star clusters is essential to properly model their gas retention and expulsion abilities in both one and three dimensions. Many models assume and rely on slow winds from the interiors of AGB envelopes to drive large amounts of stellar wind retention in the cores of young massive clusters (e.g. D'Ercole et al. 2008). However, observations of fast winds from the upper envelope layers of evolved stars complicate this picture (Mauas et al. 2006). In addition, thermalization of evolved stellar winds with the faster winds of the more numerous main sequence stars may be effective at expelling gas from stellar clusters (Smith 1999).

Adding to the complexity of the evolution of these systems is the existence of many other mechanisms beyond stellar winds that can be responsible for the deposition of mass into massive star clusters at different times in their evolutionary history. If the cluster does not form in isolation, accretion of external gas could pollute enriched material and thus change the abundance patterns of forming stars (Pfleiderer-Altenburg & Kroupa 2009; D'Ercole et al. 2010; Naiman et al. 2011; Conroy 2012). If this non-isolated cluster moves too quickly through its background medium, ram pressure stripping could remove the majority of the gas from these systems, effectively quenching star formation (Naiman et al. 2009; Priestley et al. 2011). Additionally, any low level gas produced later in the star cluster's life may be stripped from passages through its host galaxy's disk, depending on its particular orbital parameters (de Silva et al. 2009; Martell & Smith 2009; Pancino et al. 2010a).

Early in a star cluster's evolution there are a multitude of additional sources of energy injection that might be responsible for heating the intercluster gas. Both SNII and SNIa can add energy and heavy elements to a star cluster in the first tens to hundreds of Myrs of a star's lifetime, and, under certain conditions, can effectively drive all gas out of these young clusters (Krause et al. 2013), while classical novae can drive out gas in all but the most massive clusters at slightly later times (Moore & Bildsten 2011). Accretion onto compact stellar remnants is another possible avenue to clear gas rapidly in young star clusters (Leigh et al. 2013). Lyman-Werner flux serves as a means to heat intercluster gas and keep stars from forming during the first few Myrs of a star cluster's life (Conroy & Spergel 2011; Conroy 2012; Krause et al. 2013), and gas heating by UV radiation from

a population of white dwarfs serves as a possible avenue to expel intercluster gas at late times (McDonald & Zijlstra 2015). Indeed, there exists many means to expel gas from recently formed clusters to distances on the order of hundreds of parsecs (Bastian et al. 2014; Hollyhead et al. 2015).

In the work presented here we focus on predominately using stellar winds as the sole source of mass and energy in the formation of isolated star clusters and only briefly touch on the effects of extra sources of mass and energy. Throughout the majority of this paper we remain agnostic about the origin of the abundance spreads observed in present day GCs and their possible evolution from YMCs and IACs, and instead endeavor to study the role that the mass loss and energy injection from stellar winds plays in determining whether significant gas is retained or expelled from a star cluster given the cluster's mass, compactness, and age. The paper is outlined as follows: In section 2 we review our implemented hydrodynamical scheme. Section 3 describes our stellar evolutionary models generated with the MESA (Paxton et al. 2011) code, paying careful attention to the prescriptions used to describe the mass loss and wind velocities emanating from stars of different masses. This section also describes how the results for individual stars of different masses are combined into average mass and energy loss prescriptions from a population of stars, under different assumptions about the effective thermalization of winds from different stellar populations. In section 4 we present the resultant stellar wind mass retention for star clusters with a variety of masses, compactnesses and ages. Section 5 briefly discusses the effects of other heating mechanisms beyond those from stellar winds on the removal of material from star clusters and touches on the effects of different gas metallicities on the cooling properties of intercluster gas. Finally, we end with a discussion of the application of our results to gas retention and star formation in present day YMCs, IACs, and GCs presented in section 6 and summarize our conclusions in section 7.

2 HYDRODYNAMICAL METHODS AND INITIAL SETUP

To examine the ability of clusters to effectively retain the winds emanating from their evolving stellar members, we simulate mass and energy injection in isolated core potentials under the assumption of spherical symmetry (Quataert 2004; Hueyotl-Zahuanitla et al. 2010). The one-dimensional hydrodynamical equations are solved using FLASH, a parallel, adaptive mesh refinement hydrodynamical code (Fryxell et al. 2000). The winds from the closely packed stellar members are assumed to shock and thermalize such that density and energy contributions can be treated as source terms in the hydrodynamical equations.

The stellar cluster potentials are modeled as Plummer models (Brüns et al. 2009; Pfleiderer-Altenburg & Kroupa 2009)

$$\Phi_g = -\frac{GM_c}{[r^2 + r_c^2(\sigma_v)]^{1/2}} \quad (1)$$

for a given total mass, M_c , and velocity dispersion, $\sigma_v = (3^{3/4}/\sqrt{2})^{-1} \sqrt{GM_c/r_c}$. While the shape of the potential can have an effect on the radial distribution of gas inside the core (Pfleiderer-Altenburg & Kroupa 2009; Naiman et al. 2011), the overall amount of gas accumulated in the cluster is relatively unchanged by the exact form of its potential. For the sake of simplicity, we assume the potential does not change appreciably over the period of gas accumulation.

In addition to following the dynamics of the gas under the influence of Φ_g , the self gravity of the gas is computed using FLASH's

multipole gravity module. We fix our resolution to 6400 radial cells for each model, with linearly equidistant spacing between the minimum (r_{\min}) and maximum (r_{\max}) radius. The resolution within the computational domain is set by the core radius, r_c , to ensure that we are adequately resolving the core and that the cluster's potential is effectively zero at the outer boundary (cell centers are then approximately $r_{\min} \sim 0.02 r_c$, and $r_{\max} \sim 65 r_c$).

Given this potential and assuming spherical symmetry, at a time t_n , we construct the conservation of mass, momentum, and energy in a more general form starting from those in (Hueyotl-Zahuantita et al. 2010; Priestley et al. 2011):

$$\rho(r, t_n) = \rho(r, t_{n-1}) + q_m(r, t_n) dt(t_n, t_{n-1}) \quad (2)$$

$$\begin{aligned} v(r, t_n) = & v(r, t_{n-1}) \rho(r, t_{n-1}) / \rho(r, t_n) + a_g(r, t_{n+1}) dt(t_n, t_{n-1}) \\ & + p_{\text{non-uniform}}(r_{i-1}, r_{i+1}) / \rho(r, t_n) + p_{\sigma}(r_{i+1}, r_{i-1}) / \rho(r, t_n) \end{aligned} \quad (3)$$

$$\begin{aligned} \rho(r, t_n) \epsilon(r, t_n) = & \frac{1}{2} \rho(r, t_{n-1}) v(r, t_{n-1})^2 + \rho(r, t_{n-1}) \epsilon(r, t_{n-1}) \\ & - \frac{1}{2} \rho(r, t_n) v(r, t_n)^2 + q_{\epsilon}(r, t_{n-1}) dt(t_n, t_{n-1}) - Q(r, t_{n-1}) \end{aligned} \quad (4)$$

where $\rho(r, t)$, $v(r, t)$ and $\epsilon(r, t)$ are the gas density, pressure, radial velocity and internal energy density, respectively. The term $a_g(r, t)$ includes the gravitational effects of both the stellar cluster potential (Φ_g) and the self gravity of the gas. Here, $Q(r, t) = n_i(r, t) n_e(r, t) \Lambda(T, Z)$ is the cooling rate for gas with ion and electron number densities $n_i(r, t)$ and $n_e(r, t)$, and $\Lambda(T, Z)$ is the cooling function for gas at temperature T and metallicity Z . We use $\Lambda(T, Z)$ from Gnat & Sternberg (2007) for $T > 10^4$ K and Dalgarno & McCray (1972) for $10 \leq T \leq 10^4$ K.

The $q_m(r, t)$ and $q_{\epsilon}(r, t)$ terms in equations (13)-(15) are used here to mediate the total rate of mass and energy injection at a time t in a cluster's history. For N stars each with average mass loss rate **at time t of** $\langle \dot{M}(t) \rangle$ and wind energy injection rate $\frac{1}{2} \langle \dot{M}(t) \rangle \langle v_w(t)^2 \rangle$ we have

$$\dot{M}(t)_{w,\text{total}} = N \langle \dot{M}(t) \rangle = \int 4\pi r^2 q_m(r, t) dr \quad (5)$$

and

$$\dot{E}(t)_{w,\text{total}} = \frac{1}{2} N \langle \dot{M}(t) \rangle \langle v_w(t)^2 \rangle = \int 4\pi r^2 q_{\epsilon}(r, t) dr \quad (6)$$

such that $q_{\epsilon}(r, t) = \frac{1}{2} q_m(r, t) \langle v_w(t)^2 \rangle$. For simplicity, we neglect the effects of mass segregation on the positions of main sequence and evolved stars and assume $q_m(r, t) \propto n(r)$ such that $q_m(r, t) = A(t) r^{-2} \frac{d}{dr} \left(r^2 \frac{d\Phi_g}{dr} \right)$. Here, $A(t) = \langle \dot{M}(t) \rangle / (4\pi G \langle M_{\star} \rangle)$ with the average mass of a star given by $\langle M_{\star} \rangle$.

The momentum term accounting for a non-uniform distribution of stellar wind ejected momentum within the cluster, $p_{\text{non-uniform}}$ can be derived assuming the momentum flowing into (out of) the i th cell is the integral over the momentum from the sides of stars facing outward (inward) in the $i-1$ ($i+1$) cell: $d\vec{p}_{\text{non-uniform}, \pm} = \pm q_m(r_{i-1/i+1}, t) v_w dt / d\Omega \hat{r}$, where \hat{r} is the unit vector pointing radially outward from the cluster's center. This assumes the momentum flux carried by the wind from each individual star is isotropic. Integrating over the outward (inward) solid angles assuming the spherical symmetry of the individual stellar winds gives

$\vec{p}_{\text{non-uniform}, \pm} = \pm \frac{1}{2} q_m(r_{i-1/i+1}, t) v_w dt \hat{r}$. Given our expression for q_m , for the i th cell this is expressed as:

$$p_{\text{non-uniform}}(r_i) = v_w f_c [G(r_{i-1}, r_c) - G(r_{i+1}, r_c)] dt \quad (7)$$

where

$$G(r_j, r_c) = \left(1 + \frac{r_j^2}{r_c^2} \right)^{-5/2} \quad (8)$$

and

$$f_c = \left(\frac{3M_c}{8\pi r_c^3 \langle M_{\star} \rangle} \right) \quad (9)$$

The second of the extra momentum terms, p_{σ} , arises from the fact that the stars are moving, and because the distribution of stars is not uniform, this extra momentum is not distributed uniformly throughout the cluster. Following a procedure similar to deriving equation 7 with $d\vec{p}_{\sigma, \pm} = \pm q_m(r_{i-1/i+1}, t) \sigma(r_{i-1/i+1}) dt / d\Omega \hat{r}$ and $\sigma = \sqrt{GM(< r)}/r$ this momentum term can be expressed as:

$$p_{\sigma}(r_i) = \sqrt{\frac{GM_c}{r_c^3}} f_c [F(r_{i-1}, r_c) - F(r_{i+1}, r_c)] dt \quad (10)$$

where

$$F(r_j, r_c) = r_j \left(1 + \frac{r_j^2}{r_c^2} \right)^{-13/4} \quad (11)$$

Instead of $p_{\text{non-uniform}}$ and p_{σ} , many authors include an extra term in the energy equation 4 on the order of $\frac{1}{2} n(r) \sigma^2$, where σ is the velocity dispersion of the stars within the cluster and $n(r)$ is the stellar density to account for the fact that the stars are moving (Faulkner & Freeman 1977; Smith 1999; D'Ercole et al. 2008; Priestley et al. 2011). In compact clusters, this extra energy injection term heats the gas, potentially delaying star formation until enough mass has been accumulated in the central regions to cool efficiently and subsequently trigger star formation. However, including such a term without accounting for how this energy loss would slow a star's motion violates conservation of energy over the lifetime of the star cluster and therefore we do not include it here, instead relying on p_{σ} to include the effects of stellar motion in our prescription.

A final source of energy from stars orbiting within our clusters arrises from the interaction of stellar motion induced shocks and stellar winds. The energy injection rate for shocked gas of density ρ_g around a star of mass M_{\star} moving at velocity σ_v is given by $\dot{E}_s \approx (1/2) \rho_g \sigma_v^2 \mathfrak{R}$. Here, the gas interaction rate at the bow shock generated by the moving star, $\mathfrak{R} = \sigma_v \Sigma$, can be estimated from the bow shock radius of the star (Wilkin 1996), $\Sigma \approx \pi R_0^2 = \pi \dot{M} v_w / (4\rho_g \sigma_v^2)$ where \dot{M} is the mass loss from a single star at stellar wind velocity v_w . Assuming the energy injection from a star's stellar wind is given by $\dot{E}_w = (1/2) \dot{M} v_w^2$, then the ratio of injection rates can be written simply as

$$\dot{E}_s / \dot{E}_w \approx \sigma_v / (4v_w). \quad (12)$$

Thus, appreciable changes in the heating rates caused by the motion of the stars are only expected when the cluster velocity dispersion is larger than $4v_w$. For the cluster velocity dispersions discussed here, this term is negligible and thus it is not included.

Additionally, we find the p_{σ} and $p_{\text{non-uniform}}$ terms contribute to the momentum equation minimally. As both terms are proportional to q_m and either v_w or σ_v , it is expected that they should contribute to the hydrodynamics only at early times with the intercluster density, ρ_{gas} is much smaller than $q_m dt$, in clusters which can only retain

very small amounts of material ($\rho_{\text{gas}} << q_m dt$ for all time), and for very fast winds and compact clusters. For the parameters we will be concerned with in this paper we find these effects are of the order of a few percent. While both terms aid, albeit minimally, to removing material from the cluster at large radii, within the core the p_σ term contributes to funneling gas into the center of the star cluster.

Once we drop the minimally contributing momentum terms from equations (3) and (4), we revert to the equations typically seen in other works (Priestley et al. 2011; Hueyotl-Zahuantitla et al. 2010):

$$\rho(r, t_n) = \rho(r, t_{n-1}) + q_m(r, t_n) dt(t_n, t_{n-1}) \quad (13)$$

$$v(r, t_n) = v(r, t_{n-1}) \rho(r, t_{n-1}) / \rho(r, t_n) + a_g(r, t_{n+1}) dt(t_n, t_{n-1}) \quad (14)$$

$$\begin{aligned} \rho(r, t_n) \epsilon(r, t_n) = & \frac{1}{2} \rho(r, t_{n-1}) v(r, t_{n-1})^2 + \rho(r, t_{n-1}) \epsilon(r, t_{n-1}) \\ & - \frac{1}{2} \rho(r, t_n) v(r, t_n) + q_\epsilon(r, t_{n-1}) dt(t_n, t_{n-1}) - Q(r, t_{n-1}) \end{aligned} \quad (15)$$

We also neglect the effects of external mass accumulation, which can be an important source of gas when clusters reside in cool, dense ISM gas (Naiman et al. 2009, 2011; Priestley et al. 2011; Conroy 2012). In addition to ignoring shock heating of the gas caused by the motion of the stars derived in equation 12 we ignore other specific heating sources such as photoionization or supernova, but discuss the overall effects of additional energy injection in the cluster in §5.

In cases where catastrophic cooling occurs, we assume star formation is triggered if the Jeans length of the collapsing gas is smaller than the central resolution element, or if $t_{\text{cool}} \lesssim t_{\text{dyn}}$. To estimate the gas evolution during the star forming period, our cooling prescription is modified following Truelove et al. (1997) by turning off energy losses and allowing the gas to evolve adiabatically. Such a method approximates the transition of an isothermally collapsing cloud to an optically thick, adiabatically evolving protostellar cluster while forgoing the computationally expensive three dimensional radiative transfer calculations required to treat this problem accurately. Because we do not include an explicit star formation prescription, we allow such unstable regions to evolve for a few sound crossing times before halting the simulation. With this implementation, a decrease in density of approximately one order of magnitude or more occurs without the influence of cooling. While this decrease results in a significant suppression of mass accumulation within the cluster, some gas may be retained until it is either stripped by external mechanisms or displaced by supernovae from the second generation of stars, approximately 10 Myrs after they form.

3 STELLAR EVOLUTION AND MASS LOSS ON THE HR DIAGRAM

The final ingredients to be specified in our simulations are the time dependent average mass loss rates and wind velocities, which in turn determine the mass and energy injection rates, q_m and q_ϵ . Because our simulations are spherically symmetric, these rates must encompass the average mass loss properties of the stellar population as a whole.

3.1 Mass Loss Rates and Wind Velocities from Individual Stars: Prescriptions vs. Observations

To compute the individual mass loss rates, $\dot{M}(M_\star, t)$, and wind velocities, $v_w(M_\star, t)$, as both a function of the mass of the star, M_\star and its age, t , we use the MESA stellar evolution models (Paxton et al. 2011). MESA is used to follow the evolution of a grid of stellar models with $M_\star = 0.1 M_\odot - 20 M_\odot$ from ZAMS to either the white dwarf stage, end of the AGB phase, or compact object creation.

The mass and kinetic energy injection can vary by orders of magnitude throughout a star's lifetime, therefore, to constrain our MESA models we compare our calculated mass loss rates and wind velocities with observed quantities throughout the HR diagram.

3.1.1 Mass Loss Rates

The majority of mass loss from stellar winds occurs in the RGB and AGB phases of low and intermediate mass stars ($1 \lesssim M/M_\odot \lesssim 8$) making this timeframe of mass loss important to constrain. In MESA the mass loss rates during the crucial AGB phase are implemented using the wind prescription of Bloecker (1995a), $\dot{M}_B = 1.93 \times 10^{-21} \eta_B (M/M_\odot)^{-3.1} (L/L_\odot)^{3.7} (R/R_\odot) M_\odot \text{yr}^{-1}$, with a normalization of $\eta_B = 0.04$ consistent with LMC measurements (Ventura et al. 2000) and with previous studies (D'Ercole et al. 2008, 2010; Conroy & Spergel 2011). The Reimers (1975) prescription, $\dot{M}_R = 4 \times 10^{-13} \eta_R (M/M_\odot)^{-1} (L/L_\odot) (R/R_\odot) M_\odot \text{yr}^{-1}$, $\eta_R = 1.0$, is used in MESA to estimate the mass loss during the RGB branch.

In general, the mechanisms that drive mass loss during the RGB and AGB phases are not well constrained (Ventura & D'Antona 2008b; Karakas & Lattanzio 2007; Marigo 2012), and as such, it is generally unproductive to compare instantaneous mass loss rates between our models and observations. However, we can constrain mass loss prescriptions during these crucial phases by comparing the total mass lost by the MESA models with the observed the initial-final mass relation. As shown in Figure 1, we find that our models reproduce the initial-final mass relation over this key mass range.

While mass loss along the main sequence is minimal, the kinetic energy injection can be significant as will be discussed in detail in section 3.2. Therefore, to account for mass loss during this stellar evolutionary phase, we extend the Reimers (1975) prescription to mass loss along the main sequence in our MESA models - $\dot{M}_{R,MS} = 4 \times 10^{-13} \eta_R (M/M_\odot)^{-1} (L/L_\odot) (R/R_\odot) M_\odot \text{yr}^{-1}$, with $\eta_R = 1.0$. This prescription fits within the highly variable range of mass loss rates observed in main sequence stars as depicted in Figure 2.

We end this section by noting that the main sequence mass loss rate may also be estimated analytically using the typical relations between mass, luminosity and radius along the main sequence. Using the Reimers mass loss prescription and the main sequence relations of Demircan & Kahraman (1991) for luminosity, $L \simeq 1.03 (M/M_\odot)^{3.42} L_\odot$, and radius $R \simeq 0.85 (M/M_\odot)^{0.67} R_\odot$, the analytical relation for mass loss along the main sequence, $\dot{M}_{R,MS} \simeq \eta_R 3.5 \times 10^{-13} (M/M_\odot)^{3.09} M_\odot/\text{yr}$, is plotted in Figure 2. In general, the MESA relation and analytical fits are comparable, but we caution this will change based on the various iterations of the equations from Demircan & Kahraman (1991).

3.1.2 Wind Velocities

To include the full effects of the material ejected by unbound stellar winds in our simulations knowledge of not only the mass loss rates of the stars, but the amount of kinetic energy injected by winds

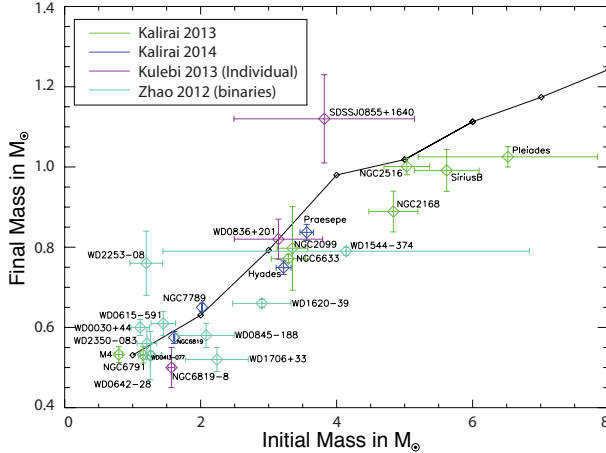


Figure 1. Initial final mass relation from observations and MESA calculations. The [Kalirai 2013](#) and [Kalirai et al. 2013](#) points are averaged over the total observed white dwarfs in each respective cluster, while the [Külebi et al. 2013](#) and [Zhao et al. 2012](#) points are taken from individual observations.

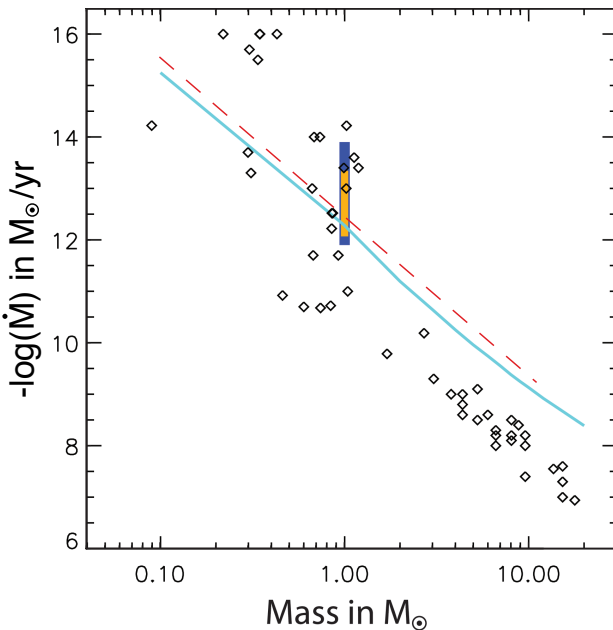


Figure 2. Mass loss rate estimates along the main sequence as a function of initial stellar mass. Observational estimates are plotted as black diamonds ([Cranmer & Saar 2011](#); [de Jager et al. 1988](#); [Searle et al. 2008](#); [Waters et al. 1987](#); [Debes 2006](#); [Badalyan & Livshits 1992](#); [Morin et al. 2008](#)). The blue rectangle denotes the estimated variations in the solar mass loss rate ([Wood et al. 2005](#)), and the yellow rectangle shows the observed variations in the mass loss rate of the Sun as a function of its X-ray activity ([Cohen 2011](#)). The blue line shows the main sequence mass loss rate prescription used by MESA and the often derived analytical prescription is shown with the dashed red line.

during different phases of evolution for each star is necessary. Here, we take the wind velocity, v_w , coupled with the mass loss rate, as a proxy for the amount of energy injected by stellar winds - $E_{\text{th,winds}} \sim \dot{M} v_w^2$. This assumption requires efficient thermalization between the stellar wind ejecta and intercluster gas. Thus, in order to proceed it is necessary to determine the velocity of stellar wind material which is unbound to the mass losing stars.

While the wind velocity can be approximated as the escape velocity, accurate within a factor of a few across a wide range of masses and life stages ([Abbott 1978](#); [Evans et al. 2004](#); [Schaerer et al. 1996](#); [Nyman et al. 1992](#); [Vassiliadis & Wood 1993](#); [Loup et al. 1993](#); [Dupree & Reimers 1987](#); [Debes 2006](#); [Badalyan & Livshits 1992](#)), in many clusters where v_{esc} for an individual star is comparable to the velocity dispersion of the cluster, a factor of two is the difference between significant mass retention in the cluster or large scale gas expulsion. To test the accuracy of the assumption of $v_w \approx v_{\text{esc}}$ we compare the predicted wind velocities from several MESA models with observations in Figure 3. $\text{H}\alpha$, Ca II H and K lines probe lower in the atmosphere and generally show outflows with velocities less than the escape velocity from the star at that depth (squares in Figure 3), while the $\text{He I } 10830 \text{ \AA}$ line is produced higher in the atmosphere and typically results in observed outward velocities comparable to the escape velocity of the star (circles in Figure 3) ([Dupree et al. 1992b](#); [Mauas et al. 2006](#); [McDonald & van Loon 2007](#); [Dupree et al. 2009](#); [Mészáros et al. 2009](#); [Smith et al. 2004](#)). Given the lack of any observed inflow and the acceleration of the material from the lower layers of the AGB and RGB atmospheres it is probable that the velocity of the outflowing material continues to increase until it reaches the escape velocity from the star ([Mauas et al. 2006](#)). Thus, the assumption $v_w \approx v_{\text{esc}}$ results in MESA stellar wind models which best reproduce the distribution of velocities lost from stars in unbound stellar winds as shown in Figure 3.

In addition to the mass lost from a star during its main sequence life time and late stages of evolution, material may be removed by close encounters with other stars ([Pasquato et al. 2014](#)), or slower moving material may be stripped from the star as it moves through the intercluster medium ([Wilkin 1996](#)). While stellar winds result in an injection of material at $v_w \approx v_{\text{esc}}$, the last two mechanisms are possible avenues for incorporating slower moving (and thus, a lower injected kinetic energy material) into the intercluster medium if the lower atmospheric layers are stripped.

One can estimate the effectiveness of ram pressure stripping on removing material from the lower atmosphere of RGB/AGB stars through the method outlined in [Wilkin \(1996\)](#) by calculating the stand-off radius of the bowshock as the star moves through the background medium:

$$R_{\text{rps}} = 8.3 \times 10^5 R_\odot \left(\frac{\dot{M}}{10^{-8} M_\odot/\text{yr}} \right) \left(\frac{v_w}{10 \text{ km s}^{-1}} \right) \left(\frac{n}{\text{cm}^{-3}} \right) \left(\frac{v_\star}{30 \text{ km s}^{-1}} \right) \quad (16)$$

For typical values of mass loss rate, $\dot{M} \sim 10^{-8} M_\odot/\text{yr}$, wind velocity, $v_w \sim 10 \text{ km s}^{-1}$, cluster velocity dispersion $v_\star \sim 30 \text{ km s}^{-1}$, and intercluster gas density $n \sim 1 \text{ cm}^{-3}$, the interaction radius is much larger than the atmospheric extent of an RGB/AGB star, $R_\star \approx 100 - 200 R_\odot$ and therefore it is unexpected that ram pressure stripping plays a significant role in the majority of gas injection within a cluster. However, as the cluster gas density increases during high mass loss, low wind velocity phases this bowshock interaction radius may penetrate to the outer layers of RGB/AGB atmospheres - a intercluster gas density of $n = 10^7 \text{ cm}^{-3}$ results in a stand-off radius of $R_{\text{rps}} \approx 200 R_\odot$.

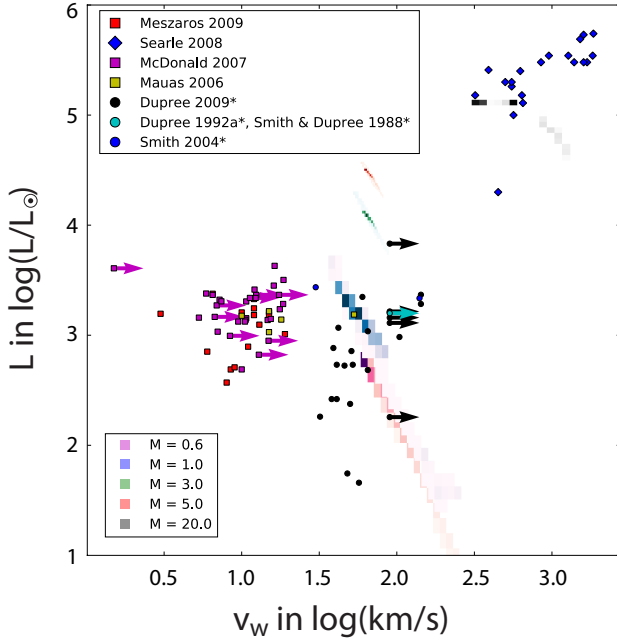


Figure 3. Luminosity and wind velocities for AGB and RGB observations and MESA models are shown here with squares and circles while observations from high mass main sequence stars are shown with diamonds. Two dimensional histograms plot the range of luminosities and wind velocities present in our MESA models, weighted by the mass lost in each bin, with the assumption that $v_w = v_{esc}$. For AGB and RGB stars, square points depict observations of outflows using H α and Ca II triplet lines (Mauas et al. 2006; McDonald & van Loon 2007; Mészáros et al. 2009) while circles show observations made with the He I $\lambda 10830$ line (Smith & Dupree 1988; Dupree et al. 1992b, 2009) which is generated higher in the atmospheres of giants (Dupree et al. 1992a). Observations noted with an asterisk denote those with a measured M_V which was converted to a luminosity for the sake of plotting. The current masses of observed AGB and RGB stars are in the range $0.6 - 1.0 M_\odot$ (Smith & Dupree 1988; Dupree et al. 1992b; Mauas et al. 2006; McDonald & van Loon 2007; Mészáros et al. 2009; Dupree et al. 2009). Masses for high mass main sequence stars range $10 \leq M/M_\odot \leq 20$ (Searle et al. 2008).

Equation 16 does not account for the non-constant nature of AGB mass loss which may result in periods of slow moving ejecta. As noted in Villaver et al. (2003, 2012) this periodic mass loss can lead to a large scale shell structure (1-2 pc) moving at slow velocities ($2 - 5 \text{ km s}^{-1}$) for AGB stars moving through the galactic ISM. However, these simulations were conducted assuming slow moving winds emitted from isolated AGB stars, conditions quite different than found in most star clusters.

While ram pressure stripping may be effective in removing low velocity gas from stars in high gas density environments, ejection of stellar material during close star encounters could be prominent in high stellar density environments (Pasquato et al. 2014). This may be an important route to include lower velocity wind material in the centers of the most dense globular clusters where interactions between stellar members is likely (Pooley et al. 2003; Pasquato et al. 2014).

In what follows we will ignore these possible secondary routes for the inclusion of stellar wind material at lower wind velocities and focus our attention on determining the effects of stellar winds alone on the mass and temperature of gas retained and ejected from star clusters.

3.2 Average Mass Loss and Wind Velocities as Model Inputs

To finalize our mass and energy injection prescriptions it is necessary to derive an averaged mass loss rate and wind velocity during each phase of cluster evolution which includes contributions from the stars that significantly contribute to the mass and kinetic energy injection into the cluster. The averaged prescription we present here has the added benefit of minimizing the effects of the poorly constrained, rapidly varying, final stages of a star's life (Pooley & Rappaport 2006).

3.2.1 The Turn Off Approximation

To estimate the net mass loss and mean thermal velocities of the colliding winds, we first follow the formalism developed by Pooley & Rappaport (2006) where the integrated wind kinetic energy and mass loss of the stellar population's turn off star is used as a proxy for the average wind velocity and mass loss rate:

$$\langle v_{w,to}^2 \rangle \approx \frac{2\Delta E_K}{\Delta M} \quad (17)$$

$$\langle \dot{M}_{to} \rangle \approx \frac{\Delta M}{\Delta t}. \quad (18)$$

where $\dot{M}_{to}(t)$ and $v_{w,to}(t)$ are the mass loss rate and wind speed of turn off stars with a mass M_\star at a particular cluster turn off time of t . Here $\Delta E_K = \frac{1}{2} \int_{t_0}^{t_1} \dot{M}_{to} v_{w,to}^2 dt$ and $\Delta M = \int_{t_0}^{t_1} \dot{M}_{to} dt$ are the kinetic energy and mass loss input rates integrated over the lifetime of the turn-off stars, $\Delta t = t_1 - t_0$, where t_0 is the zero age main sequence (ZAMS) and t_1 is the end of the AGB phase, white dwarf stage, or compact object creation. This provides a reasonable estimate for the overall wind mass and energy supply to the cluster although it fails to capture the variability of realistic stellar winds which are currently not well constrained (Marigo 2012; Wood et al. 2005; Cohen 2011).

3.2.2 The Population Averaged Approximation

The effects of the additional input of mass and kinetic energy by stars with $M_\star < M_{\star,to}$, which are neglected in the formalism previously outlined, can be included by convolving the above definitions of the average mass loss rate and wind velocity with an initial mass function (IMF) and a star formation history. Following Kroupa et al. (2013), the average number of stars in a mass interval $[M_\star, M_\star + dM_\star]$ evolving between $[t, t+dt]$ is given by $dN = \zeta(M_\star, t) N_\star b(t) dM_\star dt$ where $\zeta(M_\star, t)$ is the IMF, which we assume is accurately described by the Kroupa (2001) IMF, $b(t)$ is the normalized star formation history, and N_\star is the total number of stars. For a non-evolving IMF, $\zeta(M_\star, t) = \zeta(M_\star)$, with a mass distribution extending from masses $M_{\star,L}$ to $M_{\star,H}$, the normalized star formation history can be written as $1/t_{age}(M_{\star,L}) \int_0^{t_{age}(M_{\star,L})} b(t) dt = 1$, where $t_{age}(M_\star)$ is the lifetime of a star of a given M_\star . Examples of $b(t)$ include a constant star formation rate, $b(t) = 1$, or a coeval population, $b(t) = \delta(t - t_0)$, with all stars formed at t_0 .

The average mass $\langle \Delta M(t_i) \rangle$ and kinetic energy $\langle \Delta E_K(t_i) \rangle$ injected into the cluster environment at a time t_i , by a population of stars with $M_\star \in [M_{\star,L}, M_{\star,H}]$ where the lowest and highest mass in a population depends on both the age, t_i and the birth rate of stars, with the birth rate regulated by $b(t)$, are then given by

$$\langle \Delta M(t_i) \rangle = \int_{t_0}^{t_i} \int_{b(t_0)}^{b(t_i)} b(t) \int_{M_{\star,L}}^{M_{\star,H}} \zeta(M_\star) \dot{M}(M_\star, t) dM_\star db dt$$

and

$$\langle \Delta E_K(t_i) \rangle = \frac{1}{2} \int_{t_0}^{t_i} \int_{b(t_0)}^{b(t_i)} b(t) \int_{M_{\star,L}}^{M_{\star,H}} \zeta(M_{\star}) \dot{M}(M_{\star}, t) v_w^2(M_{\star}, t) dM_{\star} db dt, \quad (20)$$

respectively. Here, the lowest and highest masses existing at a given time depends on the current time and birth rate - $M_{\star,L}(t_i, b)$, $M_{\star,H}(t_i, b)$. Stars that have lifetimes $t_{\text{age}}(M_{\star}) < t_i$ forsake the stellar population unless they were born during the most recent star formation time interval $[t_i - t_{\text{age}}(M_{\star}), t_i]$. For this reason, t_0 is set to $\max[0, t_i - t_{\text{age}}(M_{\star})]$. This formalism allows for equations (17) and (18) to be cast into a more general form for the average mass loss rates and wind velocities at a specific stellar population life-time, t_i :

$$\langle \dot{M}(t_i) \rangle = \frac{\langle \Delta M(t_i) \rangle}{t_i} = \frac{1}{t_i} \int_{M_{\star,L}}^{M_{\star,H}} \zeta(M_{\star}) \dot{M}(M_{\star}, t) dM_{\star} dt \quad (21)$$

and

$$\langle v_w^2(t_i) \rangle = \frac{2 \langle \Delta E_K(t_i) \rangle}{\langle \Delta M(t_i) \rangle} = \langle \dot{M}(t_i) \rangle^{-1} \int_{M_{\star,L}}^{M_{\star,H}} \zeta(M_{\star}) \dot{M}(M_{\star}, t) v_w^2(M_{\star}, t) dM_{\star} dt. \quad (22)$$

In which we have assumed the stellar population initially residing in star clusters is coeval such that $b(t) = \delta(0)$, which provides an accurate description for clusters with $t_i \gtrsim 10$ Myrs.

Figure 4 compares mass loss rates and wind velocities of the the turn-off (TO) and population averaged (MS+TO) prescriptions with the instantaneous $\dot{M} - v_w$ curves for several MESA stellar evolution models. While remaining similar in mass loss rates, the effects of the additional kinetic energy contribution in the population averaged prescription compared to the turn-off prescription are evident in the overall higher wind velocities in the TO curves of Figure 4.

In what follows we will explore the effects of substituting the mass loss prescriptions described in equations 18 or 21 and the wind velocity prescriptions defined in equations 17 or 22 on a cluster's overall mass loss and kinetic energy injection as defined in 5 and 6, respectively.

4 STELLAR WIND RETENTION IN STAR CLUSTERS

The mass injection properties, characterized here by the mass loss rates and wind velocities emanating from a coeval population of stars, change dramatically as the population evolves. Figure 5 shows the evolution of the average stellar wind parameters. As the wind velocities and stellar mass loss rates change, so does the ability of a cluster potential to retain the shocked stellar wind gas. Figure 5 clearly illustrates the differences between efficient (population averaged prescription which includes the kinetic energy injected by main sequence stars) and inefficient (turn off mass prescription which does not include the kinetic energy injected by main sequence stars) thermalization and mixing of stellar winds from stars of different masses. Note that the differences between the turn off mass and population averaged prescriptions manifest themselves predominately in the values of the population's averaged wind velocity as main sequence stars do not contribute to the total mass injection rate.

Figure 5 depicts the wind properties as a function of time throughout the cluster's evolution. If the cluster has its gas removed by, for

(19)

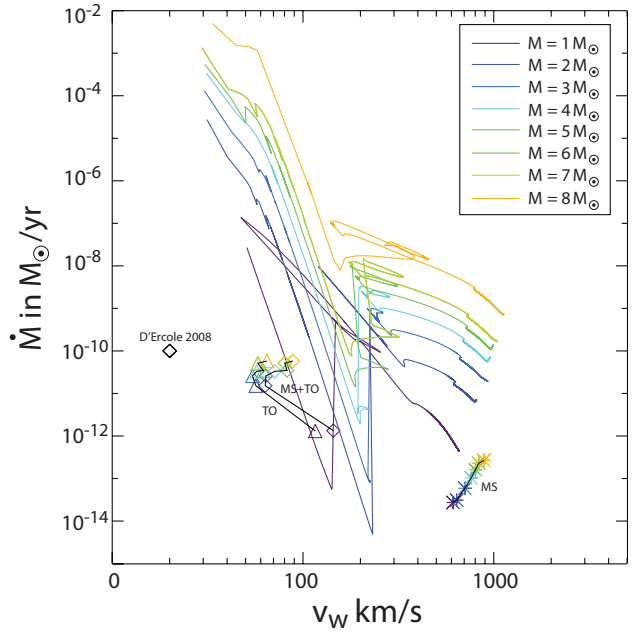


Figure 4. Mass loss rate and wind velocity for intermediate mass stars from MESA. The average mass loss per star on the main sequence alone, using the turnoff mass prescription, and using the population averaged prescription are shown with colored stars (MS), triangles (TO) and diamonds (MS+TO), respectively. For reference, the average mass loss per star from (D'Ercole et al. 2008) is shown by a black diamond at their AGB wind velocity of 20 km/s.

example, ram pressure stripping due to interaction with external gas (Priestley et al. 2011) or by additional gas heating processes, gas retention will commence without memory of any previous episode of mass accumulation. If however, the cluster potential is assumed to be non-evolving and isolated with no additional heating sources operating other than stellar winds, there will be some residual gas and the gas retention properties at a particular age will depend on the mass and energy injection history of the stellar members. We refer to these two extreme scenarios as mass retention without memory and with memory, respectively.

A young cluster without gas retention memory, corresponding to time A in Figure 5, with its high average wind velocity cannot retain gas effectively if $\sigma_v \ll v_w$. This is clearly seen in Figure 6 which shows the properties of the shocked stellar wind gas confined to a cluster potential characterized by $\sigma_v = 30$ km/s and $M_c = 10^7 M_{\odot}$ for both turn off mass and population averaged prescriptions (red curves). The flow in this case was evolved for $t_i = t_A = 23$ Myrs as the average mass loss rates and wind velocities do not change appreciably over this time period. A young cluster is thus only able to retain a small quantity of high temperature gas in its inner region ($M_{\text{acc}}/M_c \approx 10^{-7}$), while further away gas is blown out of the system in a wind.

As the cluster members evolve a dramatic decrease in the average wind velocity occurs due to the dominant contribution of the slow, dense AGB winds to the overall mass injection, corresponding to time B in Figure 5. For the star cluster, here assumed to be characterized by a non-evolving gravitational potential, the AGB contribution results in stellar wind injection parameters that favor significant mass retention, as shown in Figure 5 (black curves). As the stellar wind gas shocks and cools, mass is efficiently accumulated ($M_{\text{acc}}/M_c \approx 0.04$) until the central region becomes Jeans unstable, thus triggering star formation. In this case, the gas flow within the cluster is evolved

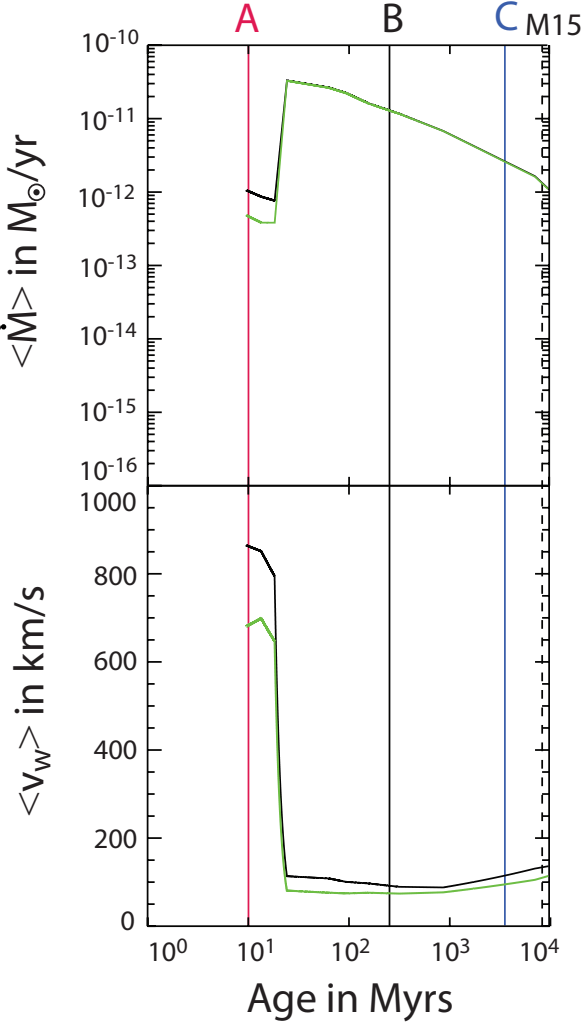


Figure 5. Average cluster mass loss rates and wind velocities as a function of time for $Z = 1/10 Z_\odot$. Green lines assume gas dynamics are dominated by the wind properties of the turn off stars (§3.2.1), black lines show the population averaged values (§3.2.2). Three representative times in the clusters age are denoted by the solid vertical lines. The current age of M15 is denoted by the vertical dashed line. Note that while the turn off stars contribute the majority of the mass (top panel), the main sequence stars dominate the energy injection (bottom panel) as a result of their higher effective wind velocities.

until $t = t_{\text{sf}}$, defined here as the sound crossing time within the (adequately resolved) Jeans unstable region. Here $t_{\text{sf}} = 1200$ Myrs and 1700 Myrs for the turn-off mass prescription and population averaged approximation, respectively.

As the cluster ages, remaining stars no longer pass through an extended thermally pulsing AGB phase. This results in a increase in average wind velocity, and decrease in average mass loss rates (by a factor of ~ 1.3 and approximately an order of magnitude over ~ 2 Gyrs, respectively) as seen at time C. As a result, the cluster potential is unable to effectively retain the emanating gas and the remaining wind material flows out of the cluster almost unrestrained ($M_{\text{acc}}/M_c \approx 10^{-7}$).

The amount of gas in clusters in which stellar wind material is efficiently retained, as in time B of Figure 5, can increase significantly if, prior to this time, the cluster is not stripped of gas prior to this time by additional internal heating sources or by external gas removal. In this case the cluster can retain the memory of previous

gas accumulation. Figure 7 compares the hydrodynamical profiles and central gas mass accumulation histories of two clusters in which mass retention is assumed to take place with and without memory. In both cases, star formation is triggered albeit at different times and involving different amounts of accumulated cold gas. The larger central gas density in the model with memory and residual gas results in a few percent increase in cold gas made available for a second generation of star formation - M_{acc}/M_c increases from 4.3% to 6.9% when the mass retention takes place with memory.

The ability for a star cluster to retain wind ejecta depends not only on the evolutionary stage of its members but also on their spatial distribution. To illustrate this, in Figure 8 we show the properties of the shocked stellar wind gas confined to a shallow potential characterized by $\sigma_v = 14$ km/s and $M_c = 4.5 \times 10^5 M_\odot$ (parameters thought to accurately represent the current stellar mass distribution in the globular cluster M15 (McNamara et al. 2004; Gerssen et al. 2002)). A shallow gravitational potential is thus unable to retain a significant amount of stellar wind material, even during the AGB phase. This is observed to also be the case in simulations in which the cluster is assumed to have gas retention memory.

The dramatic difference observed in Figures 6 - 8 between the stellar wind mass accumulated in cluster potentials of varying properties motivates our study to compare results obtained with different velocity dispersions and cluster masses for clusters with and without gas retention memory. To facilitate comparisons, we first systematically vary the cluster velocity dispersion for a fixed total mass $M_c = 10^7 M_\odot$, assuming the turn off mass wind velocity and mass loss rate are representative of the entire population and the cluster has no gas retention memory. The left panel of Figure 9 gives the amount of accumulated stellar wind mass in units of M_c for a range of cluster velocity dispersions and different evolutionary stages (t_i) of the stellar members. By looking at the shaded regions in Figure 9, the reader can identify the cluster velocity dispersion and mass combinations for which favorable conditions for star formation are satisfied at a given cluster age provided there is no memory of gas retention.

Cluster potentials with $\sigma_v \lesssim 20$ km/s are not effective at retaining gas in their cores, and gas is blown out of the cluster at all times. As the velocity dispersion increases above 30 km/s, the cluster core is able to retain the shocked and efficiently cooled stellar wind gas, making the central region Jeans unstable before (i.e. $t_{\text{sf}} \ll t_i$) a significant amount of mass is accumulated into the cluster. The largest fraction of mass retained takes place for star clusters with $\sigma_v \approx 25$ km/s. In this case, the potential is steep enough to retain the shocked and subsequently cooled wind material, but shallow enough to force the cold gas to collapse only until a significant amount of mass has been accumulated. The contours in the left panel of Figure 9 show that potentials with $\sigma_v \gtrsim 30$ km/s may endure multiple episodes of star formation albeit involving less retained gas, while potentials with $25 \text{ km/s} \lesssim \sigma_v < 30 \text{ km/s}$ can have only short but more intense star formation periods. However, because we do not treat star formation explicitly, future detailed simulations are needed to address the possibility of recurrent star formation in these systems. The largest mass accumulation for a single star formation episode occurs for $\sigma_v \approx 27$ km/s between the ages of 1 – 10 Gyrs, with a mass retention fraction of $M_{\text{acc}}/M_c \approx 6.4\%$.

The extension of the star formation region in Figure 9 depends dramatically on the velocity dispersion of the cluster. While our optimal single star formation episode takes place between cluster ages of 1 – 10 Gyrs, significant levels of star formation can occur at earlier times for higher velocity dispersions - clusters with younger

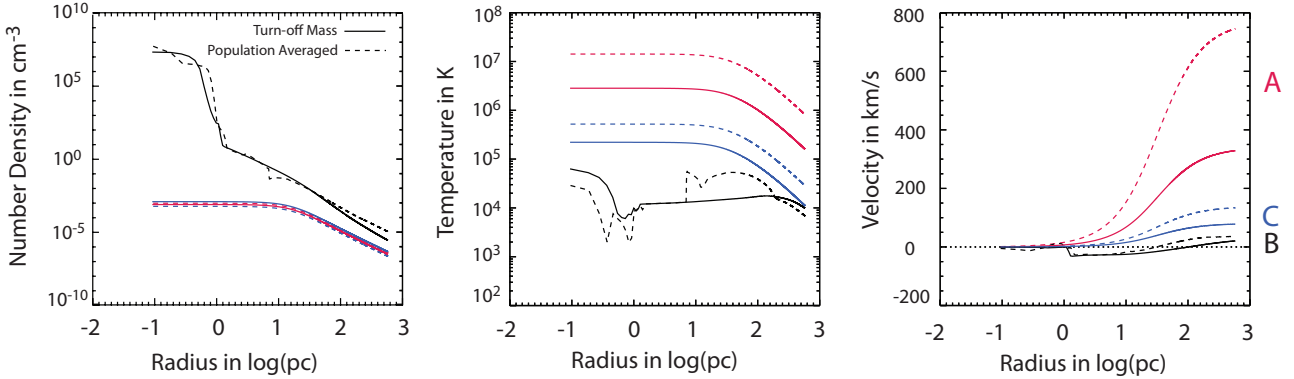


Figure 6. Hydrodynamic profiles for the three representative times, A(red), B(black) and C(blue), as denoted in Figure 5. These three plots are the density, temperature and velocity profiles at three representative times for a $M_c = 10^7 M_\odot$, $\sigma_v = 30 \text{ km/s}$ model. Solid and dashed lines represent the turn off mass and population averaged prescriptions for models without memory, respectively.

ages, $\approx 200 - 400$ Myrs, can retain approximately 3% of the original cluster mass provided $\sigma_v \gtrsim 30 \text{ km/s}$.

For consistency with other works we have repeated our analysis shown in right panel of Figure 9 including the effects of the cluster velocity dispersion term which is often added to the energy relation derived in equation 15. For brevity, the contour map is not included here but we note that we find that in compact clusters this extra energy injection term slightly delays star formation until enough mass has been accumulated in the central regions to cool efficiently and subsequently trigger star formation. However, for less compact clusters ($\sigma_v \lesssim 35 \text{ km/s}$) this additional heating is not important.

The right panel of Figure 9, in conjunction with the left panel, allows us to estimate the amount of stellar wind material retained by a star cluster of a given age, mass and velocity dispersion. While our models do not span the full range of $M_c - \sigma_v$ combinations, some generalizations can be made from the results presented in Figure 9. The conclusions drawn are based upon the assumption that the cluster potential properties, whose evolution causes are poorly known, remain relatively unaltered for $\min[t_i, t_{sf}]$ and that the cluster has no gas retention memory. The right panel of Figure 9 is self-explanatory - heavier star clusters at a fixed velocity dispersion retain more gas. The mass retention fraction is observed to increase slightly with augmenting cluster mass as a result of less efficient cooling, which in turn delays the triggering of star formation as mass continues to accumulate. Depending on how the cluster evolves, the assumption of a static potential used in Figure 9 may break down, however the effects of a time varying potential can be estimated by altering the trajectory of a cluster in the $[\sigma_v, \text{time}]$ or $[M_c, \text{time}]$ plane.

Using the average wind velocity and mass loss rate of the turn off mass star alone to represent the properties of the entire population underestimates the kinetic energy input arising from the more numerous, lighter stars (Figure 5). This gives an optimistic value of the wind retention and star formation efficiencies. The effects of using the total kinetic energy input from the star cluster, including the contribution from the main sequence stars, to calculate effective mass retention are shown in Figure 10. Direct comparison with Figure 9 shows that although the overall mass accumulation is rather similar, in the population-averaged prescription star formation is triggered over a narrower range of velocity dispersions. Not only are higher velocity dispersions required to produce efficient star forming models, but the additional kinetic energy inhibits star formation in the largest mass accumulation regions. This is because the larger wind velocities keep the gas at higher temperatures, thus quenching star

formation. Previous studies used the instantaneous AGB wind velocity as proxy for the total kinetic energy being injected into the cluster. Our results suggest that the inclusion of the kinetic energy provided by the main sequence stellar winds can dramatically alter the gas dynamics in these systems. However, the ability of stellar winds from different populations to mix and effectively thermalize remains uncertain and a clear understanding of their combined effects will require detailed multidimensional simulations, which are currently beyond the scope of this paper.

The effects of additional kinetic energy injection by main sequence stars in star clusters can be mitigated by the larger densities and thus enhanced cooling rates present in models where gas retention is allowed to proceed unimpeded throughout the cluster's evolution. Figure 11 depicts the effects of gas retention with memory on the central mass accumulations and star formation histories of a $M_c = 10^7 M_\odot$ cluster for a variety of velocity dispersions. Note that our rudimentary treatment of star formation prevents us from following the gas evolution once star formation has been triggered, resulting in an incomplete coverage of the $M_c - \sigma_v$ plane in Figure 11. In Figure 11, the largest mass accumulation coincides with the lower σ_v bound of the star formation region. The continuous accumulation of gas also produces larger central gas masses, with a gas mass of up to 9% of the cluster's mass retained. A comparison between the mass accumulation contours in Figure 11 with those in the left panel of Figure 9 should provide the reader with some understanding of the importance of gas retention memory although such comparison should be done with care, as the assumption of a non-evolving potential in Figure 11 is not necessarily a good approximation over a large expanse of time.

In estimating the effects of star formation episodes in Figures 9 - 11, we assume that such events do not effect the average stellar mass loss parameters dramatically. This approximation will hold true provided that number of stars form during these episodes is small, as suggested by our work. In such cases, the shaded regions depicted in Figures 9 - 11 provide valid constraints on the star formation ages and masses expected from stellar wind retention.

5 FURTHER CONSIDERATIONS

Throughout this work, we have used simplified models to determine how effective a star cluster of a particular age is at retaining gas emanating from its stellar members, under the assumption that its potential remains unaltered during the simulated phase. We have

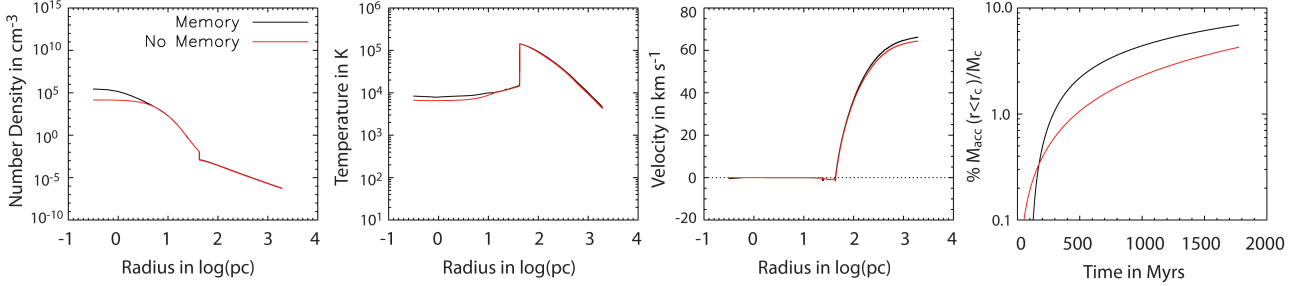


Figure 7. Hydrodynamic profiles and gas accumulation for a $t_i = 2000$ Myrs cluster with $M_c = 10^7 M_\odot$ and $\sigma_v = 27$ km/s. When the cluster is allowed to retain residual gas throughout its evolution (black line) it can accumulate significantly more mass (6.9% instead of 4.3%) by the time star formation is triggered than when the cluster is assumed to have no retention memory.

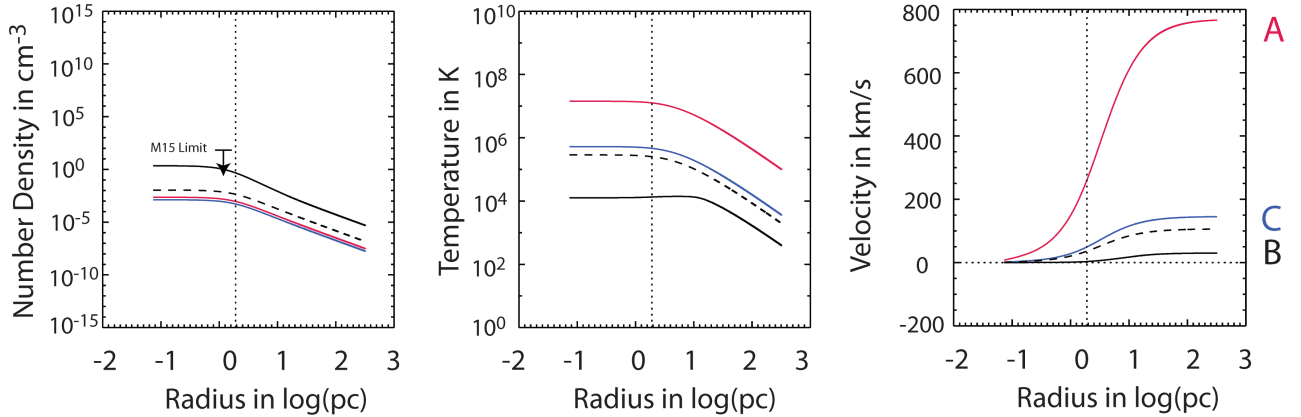


Figure 8. Hydrodynamic profiles for M15 with $M_c = 4.5 \times 10^5 M_\odot$ and $\sigma_v = 14$ km/s (McNamara et al. 2004; Gerssen et al. 2002) at the three representative times in Figure 5, including the predicted profiles for its current age (dashed lines). Here, the population averaged prescription is used and we assume the cluster has no gas retention memory.

further assumed a single metallicity for all clusters and have disregarded any heating sources besides the stellar winds themselves. In this section we relax both of these assumptions.

5.1 Metallicity

Not all clusters will have stars which expel wind material at $1/10 Z_\odot$. Cluster to cluster variations in light element abundances are commonly observed in Galactic globular clusters (Beasley et al. 2005; Caldwell et al. 2011; Gratton et al. 2004; Carretta et al. 2010b; Cohen et al. 2005; Piotto et al. 2007), with spreads in heavier elements present in the most massive Galactic globular clusters (Marino et al. 2009; Carretta et al. 2009c; Ferraro et al. 2009; Carretta et al. 2010a,b). Additionally, Galactic globular clusters have metallicities which vary from cluster to cluster - [Fe/H] ranges from approximately -0.5 to -2.5 (Harris 1996), and there is evidence these metallicity variations extend to other galaxy and globular cluster systems (Usher et al. 2015). In addition, there are some observational hints at the existence of complex abundance patterns in younger clusters as well (Li et al. 2016; Martell et al. 2013). While it is not clear how robust this effect is within all young and intermediate age clusters (Mucciarelli et al. 2008; Mucciarelli 2014), there are many examples of YMCs and IACs with metallicities not equal to that in our assumed models, $Z = 1/10 Z_\odot$ (Mucciarelli et al. 2008).

These variations may cause changes in the mass loss histories of the individual stellar members and the cooling properties of the shocked gas. As the stellar mass loss prescription are mostly independent of

metallicity during the evolutionary time periods that are conducive to star formation (0.1 Gyrs $\lesssim t_i \lesssim 100$ Gyrs) (Reimers 1975; Bloecker 1995b), we account for the effects of varying metallicity solely in the cooling function. We further assume all changes are factors of solar metallicity - only an approximation when enrichment follows the abundance variations seen in present day globular clusters.

Figure 12 shows the effects of changing metallicity for a young, massive and compact star forming cluster, described here by $M_c = 10^7 M_\odot$, $\sigma_v = 50$ km/s, and $t_i = 212$ Myrs. For lower metallicities, the cooling becomes less efficient and more material is allowed to flow into the center of the cluster before catastrophic cooling occurs. This enables relatively more massive star forming episodes to be triggered. Interestingly, when metallicity is lower than $Z < 10^{-1}$, the cooling becomes weak enough to prevent catastrophic cooling at times $\leq t_i$. These results suggest that the range of cluster parameters over which large central densities will persist before catastrophic cooling takes place (Figures 9 - 11) will depend on the metallicity of the emanating stellar winds, though, as illustrated in Figure 12, the differences are not marked.

5.2 Intercluster Heating Sources

In addition to altering the cooling curves, the inclusion of additional cluster heating sources may prevent effective gas retention in our simulations. We address this problem here by artificially increasing the energy input rate: $q_{\epsilon,\text{new}} = (1 + H)q_\epsilon = (1 + H)\frac{1}{2}q_m(r)v_w^2$. Under this assumption, the additional heating sources follow the

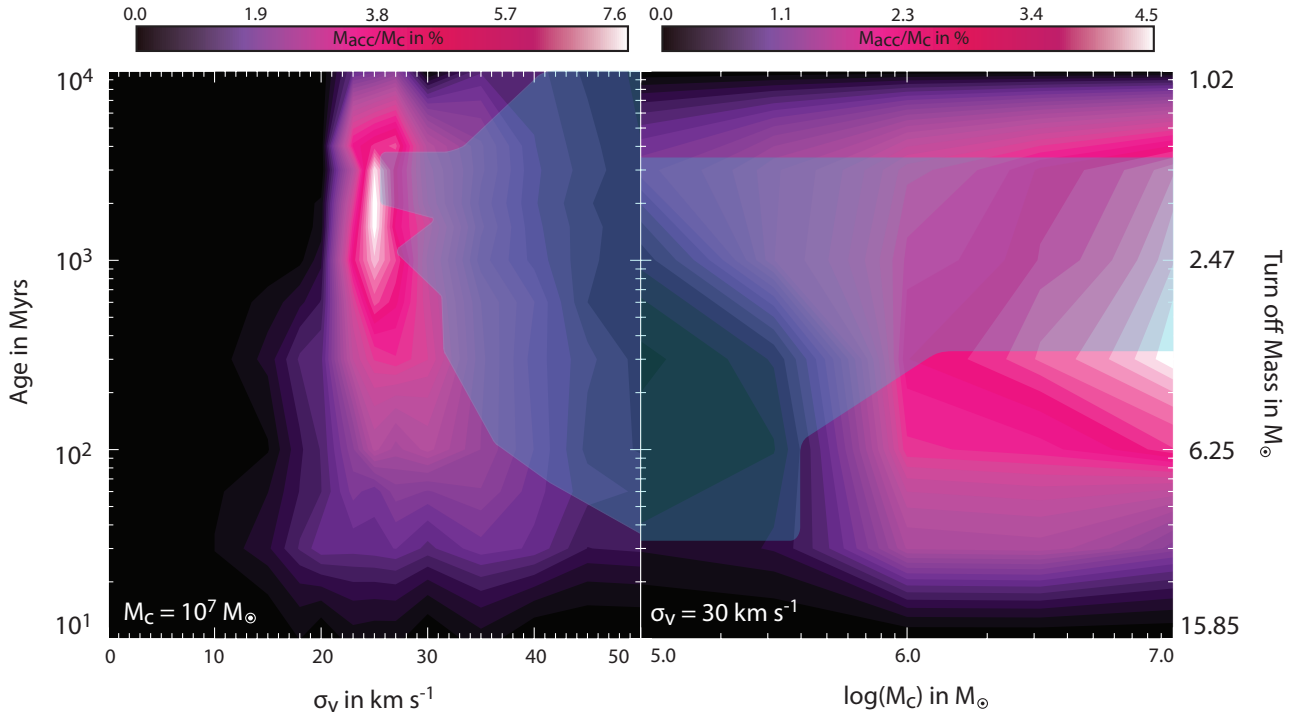


Figure 9. Mass accumulation, M_{acc} , as a function of the potential parameters M_c and σ for the turn off mass prescription. The blue shaded regions delimit the boundaries for which our models collapse and trigger star formation. *Left:* Contours of M_{acc}/M_c for a fixed cluster core mass of $M_c = 10^7 M_\odot$ and a varying velocity dispersion. *Right:* Contours of M_{acc}/M_c for a fixed velocity dispersion of $\sigma_v = 30 \text{ km s}^{-1}$ and varying cluster mass. Here we assume the cluster has no gas retention memory.

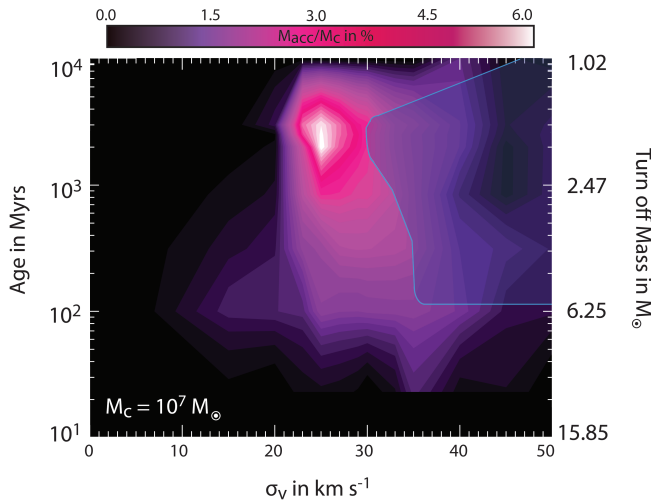


Figure 10. Mass accumulation, M_{acc} , as a function of σ_v for a fixed cluster core mass of $M_c = 10^7 M_\odot$, calculated using the population averaged prescription. The blue shaded region delimits the boundaries for which our models collapse and trigger star formation. Here we assume the cluster has no gas retention memory. The additional thermalized high velocity winds from main sequence stars add appreciable heat to the central regions of the cluster, thus inhibiting star formation at lower cluster velocity dispersions.

potential's stellar distribution. Such a heating source could be, for example, the result of including the extra velocity dispersion term to the energy relation shown in equation 15 by setting $H \approx 1$.

Figure 13 shows the effects of the additional heat input in one of

our otherwise star forming simulations. For $H < 2.0$, the gas in the simulation still collapses, triggering star formation. For larger values, on the other hand, the cluster is unable to effectively retain the gas and, as a result, star formation never ensues. By integrating $q_{\epsilon,\text{new}}$ over the cluster's core for $H = 2.0$, we derive the total energy input rate required to overturn the central mass build up, which for this simulation is about $10^{35} \text{ ergs}^{-1}$.

In many cases, the additional energy injection sources might not follow the stellar distribution. As an example, let's compare the heat distribution expected from accreting neutron stars under the assumption that the accretion feedback is proportional to the Bondi accretion rate: $q_{\epsilon,\text{ns}} \propto \dot{M} \propto \rho(r)T(r)^{-3/2}$ (Bondi & Hoyle 1944). Using the volume-averaged density and temperature in the cluster core, $\bar{\rho} \approx 10^{-22} \text{ g cm}^{-3}$ and $\bar{T} \approx 10^4 \text{ K}$, we derive the average luminosity of a single, accreting neutron star: $L_{NS} \approx 10^{33} \text{ ergs s}^{-1}$. This implies that $\gtrsim 100$ accreting neutron stars are required to reside in the cluster's core in order to significantly offset its cooling properties. However, to accurately test this phenomena a multi-dimensional approach would be required as feedback would not necessarily act as a simple heating prescription.

6 APPLICATIONS TO VARIOUS STAR CLUSTERS

We have thus far kept our discussion of stellar wind retention in star clusters generalized to star clusters with different combinations of ages, masses and velocity dispersions. In what follows we discuss the implications of gas retention on three specific groups of star clusters - Young Massive Clusters, Intermediate Age Clusters, and Globular Clusters - and provide limits on how stellar wind retention can effect their star formation histories.

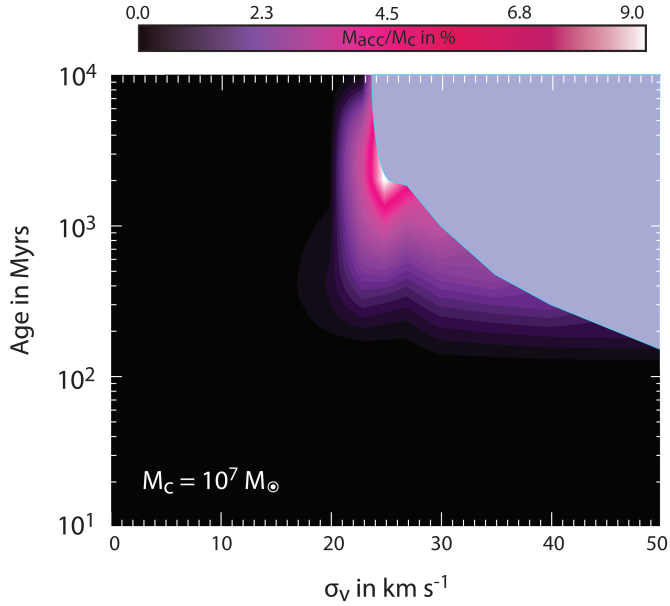


Figure 11. Mass accumulation, M_{acc} , as a function of σ_v for a fixed cluster core mass of $M_c = 10^7 M_\odot$, calculated using the population averaged prescription. The blue shaded region delimits the boundaries for which our models collapse and trigger star formation. Here we assume the cluster has gas retention memory. After star formation is triggered we expect the subsequent gas accumulation after supernova energy injection to initially proceed as in Figure 9. Here, the additional mass input increases the cooling capacity of the cluster gas when compared to that in Figure 10 and, as found previously, the star forming contours overlap with the largest central mass accumulation regions, as in Figure 9.

6.1 Young Massive Clusters: Age $\lesssim 1$ Gyr

Young, massive star clusters (YMCs) are ubiquitous in the nearby Small and Large Magellanic Clouds (Goudfrooij et al. 2014) and are also found in recent ($\lesssim 1$ Gyr) mergers like the Antennae galaxies (Whitmore et al. 2007). As one of the candidates for proto-Globular Clusters, the gas content and star formation histories of these objects are a subject of much interest (e.g. Portegies Zwart et al. 2010).

6.1.1 Current Gas Content

During the time span of the typical ages of YMCs (10s-100s Myrs) Figures 9 - 11 show little mass retention and star formation in all but the most compact stellar clusters. This results from the fast winds from main sequence O and B stars as shown in Figure 5 for ages $\lesssim 20$ Myrs, and the lack of sufficient gas accumulation time to initiate runaway cooling and collapse for clusters with $20 \lesssim \text{age/Myrs} \lesssim 500$. For clusters with large velocity dispersions, $\sigma_v \gtrsim 35 \text{ km s}^{-1}$, while some gas mass is retained and star formation is triggered, less than $\approx 2\%$ of the original cluster's mass is available for star formation.

In such clusters we expect several additional mechanisms to add significantly to the energy injection rate in the intercluster gas. As shown in Calura et al. (2015) SNe can be an effective avenue to assist in the removal of gas from stellar clusters, though in some systems SNe alone may not be able to fully remove gas from young clusters (Krause et al. 2013). In addition, accretion onto compact objects may be able to clear gas within YMCs on time scales as small as 10 Myrs (Leigh et al. 2013). Finally, Lyman-Werner flux from massive stars

further inhibits star formation by dissociating molecular hydrogen in these young systems (Tenorio-Tagle et al. 1986; Conroy & Spergel 2011; Krause et al. 2013). Therefore, we conclude that our estimates of gas retention on the order of a few percent are upper limits for the total mass retained from stellar wind ejecta within YMCs.

Such a small amount of gas retention is broadly consistent with both observations and more complex simulations. Recent observations which show little gas in all but the most compact clusters (Bastian & Strader 2014; Cabrera-Ziri et al. 2015; Kruijssen 2015; Longmore 2015), though observations at high redshift are challenging (Longmore 2015). Our results are also consistent with analytic and three dimensional simulations of which find that the majority of gas mass is removed by 1 – 14 Myrs (Calura et al. 2015; Kruijssen 2015).

6.1.2 Previous and Ongoing Star Formation

Our results of little to no star formation in Figures 9 - 11 over the several hundreds of Myrs timespan are broadly consistent with the results of Bastian et al. (2013b) which show no ongoing star formation in 130 YMCs with masses ranging from $10^4 < M/M_\odot < 10^8$ and ages $10 < \text{age/Myrs} < 1000$ and Martocchia et al. (2018) who only find MSPs in clusters with ages $\gtrsim 2$ Gyr, though our level of predicted star formation may be too low to be detectable in the majority of YMCs (Peacock et al. 2013). Our limit of $\sigma_v \gtrsim 35 \text{ km s}^{-1}$ is a slightly higher limit for velocity dispersion than that derived observationally from assuming eMSTO features in IACs (Goudfrooij et al. 2014) are due to an age spread. Such a discrepancy can be alleviated if assumed evolution of the velocity dispersion changes more dramatically from YMC to IAC stage than assumed in Goudfrooij et al. (2014) or if the eMSTO feature is due to a population of rapidly rotating main sequence stars (Cabrera-Ziri et al. 2016; Bastian et al. 2016; Piatti & Bastian 2016) or other stellar evolutionary affects (Bastian & Lardo 2017). While Li et al. (2016) see evidence for past star formation in IACs which are less massive and more diffuse clusters than predicted by our simulations, their suggestion that these episodes of star formation may have been triggered by the accumulation of gas from the clusters as they orbited within the gaseous disk of their host galaxy is not necessarily inconsistent with this work as we assume our stellar wind material is accumulated in star clusters in isolation. Previous work has shown that cold gas accretion may indeed be a viable avenue for significant gas retention and star formation (Naiman et al. 2009; Conroy et al. 2011; Conroy & Spergel 2011; Priestley et al. 2011; Naiman et al. 2011; Conroy 2012), however our detailed treatment of the interplay between these two gas accumulation processes is left to a subsequent paper.

6.1.3 Relationship to Evolved Stellar Clusters

Abundance variations of light elements in main sequence stars (Gratton et al. 2001; Briley et al. 2002; Cohen et al. 2002; Cannon et al. 1998; Pancino et al. 2010b) and RGB stars (Sneden et al. 2004) within the majority of Galactic globular clusters suggest a complex enrichment history during star formation. Our results pose problems for many of the current scenarios for explaining the complex star formation histories observed in many globular clusters under the assumption that currently observed YMCs will eventually evolve into systems like Galactic globular clusters.

Of the several scenarios attempting to explain abundance variations in globular clusters, many rely on a first generation of stars polluting the interstellar gas with enriched material which is then

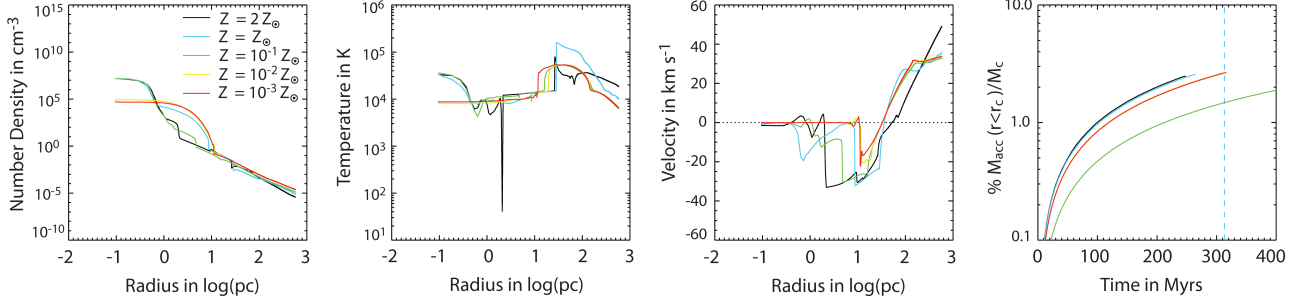


Figure 12. Gas properties for $M_c = 10^7 M_\odot$, $\sigma_v = 30 \text{ km/s}$ cluster at $t_i = 313 \text{ Myrs}$ for different metallicities. Here, we use the population averaged values of the wind parameters and assume the cluster has no gas retention memory.

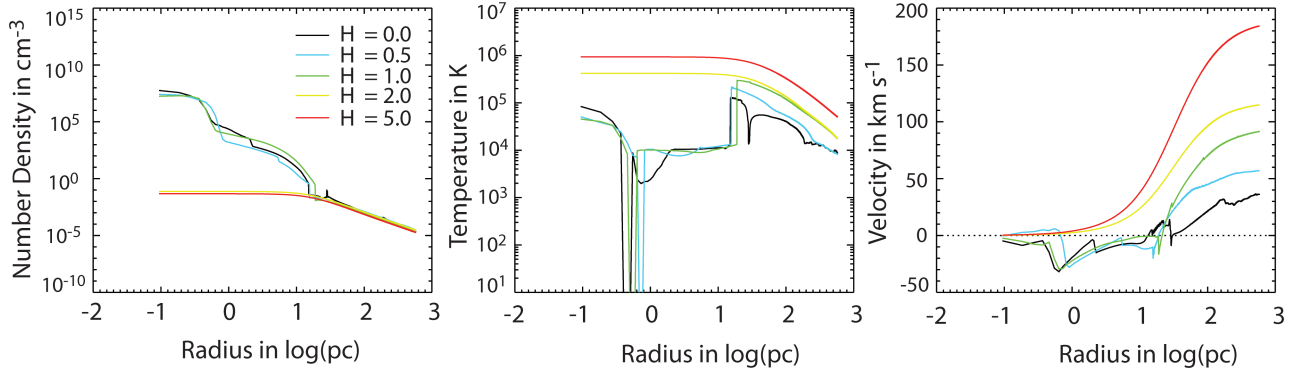


Figure 13. Left 3 Plots: Gas properties for $M_c = 10^7 M_\odot$, $\sigma_v = 30 \text{ km/s}$ cluster at $t_i = 1860 \text{ Myrs}$ with added heat in the form of thermal energy: $e_{int,new} = (1 + H)e_{int,old}$. Here, we use the population averaged values of the wind parameters and assume the cluster has no gas retention memory.

incorporated into a subsequent generation of stars. One of the more popular scenarios which may meet these requirements is enrichment from a combination of intercluster gas from the winds of AGB stars and accreted unprocessed material (Prantzos et al. 2007; Ventura & D'Antona 2008a,b; Pfleiderer-Altenburg & Kroupa 2009; D'Ercole et al. 2010; Conroy et al. 2011). The proposed timeline for this method proceeds from an initial episode of star formation into an initial clearing of gas from SNe (D'Antona & Caloi 2004; D'Ercole et al. 2008; Conroy et al. 2011). Winds from AGB stars are then effectively retained within the proto-GC, mix with an accumulation of pristine gas accreted from the cluster's surroundings, and form a subsequent population of stars. As the possible mass lost from AGB stars has an upper limit of approximately 10% of the initial mass of the cluster, a stellar mass loss of approximately 90% of the initial population of stars is invoked in order to explain the roughly equal masses of first and generation stars observed in present day GCs (D'Ercole et al. 2008; Conroy et al. 2011; Conroy & Spergel 2011; Conroy 2012).

Typically it is assumed the optimum time for retention of anomalous material is $\sim 50 - 300 \text{ Myrs}$ during which material from stars in a mass range of $4 \lesssim M/M_\odot \lesssim 8$ necessary to reproduce the abundance ratios is injected into the cluster (Ventura et al. 2001; Karakas & Lattanzio 2007; Ventura & D'Antona 2008a,b) and be consistent with the $\lesssim 1 \text{ Gyr}$ age spreads between the enhanced and unenhanced populations currently observed in globular clusters (Larsen et al. 2011; Cabrera-Ziri et al. 2014, 2016; Martocchia et al. 2018). Our results are in conflict with this scenario as we find only minimal ($\lesssim 2\%$) gas retention within the star clusters in the age range conducive to reproducing the abundance anomalies in the AGB scenario. However, it is possible the optimum time range for pollution with material enriched

by the necessary AGB stars may be modified given the differences between abundance ratios produced by different AGB models (Fenner et al. 2004; Karakas et al. 2006; Choi & Yi 2008; Bekki et al. 2007; Ventura & D'Antona 2008a,b; Doherty et al. 2014a,b).

Previous studies have shown greater gas mass retention is possible within YMCs in the proposed $\sim 50 - 300 \text{ Myrs}$ time span (D'Ercole et al. 2008, 2011; Bekki 2011), however a smaller wind velocity and different star formation prescription was used in these calculations. We compare our mass loss and wind velocity prescription with the values derived from the work of D'Ercole et al. (2008) in Figure 14. While the overall mass accumulation rate is smaller than in their work ($\sim 3 - 4\%$ vs their $\sim 10\%$), we still find discrepancies in accumulation from the difference between assumed mass loss and wind velocity prescriptions. The gas accumulation for the turn off prescription (labeled "TO" in Figure 14) is a factor of a few less than that in the D'Ercole $\dot{M} - v_w$ model, and the even lower rates observed from the population averaged prescription ("MS" in Figure 14), the latter never cooling enough to trigger star formation in our models.

Other scenarios proposed to explain the different abundances of subpopulations within present day GCs rely on complex star formation histories during a much smaller time range ($\sim 10 - 50 \text{ Myrs}$) to explain the abundance anomalies observed in present day globular clusters (Maeder & Meynet 2006; Prantzos & Charbonnel 2006; Decressin et al. 2007a,b; Charbonnel et al. 2013; Krause et al. 2013; Bastian et al. 2013a; Cassisi & Salaris 2014; Hénault-Brunet et al. 2015; Milone et al. 2016; Bastian et al. 2016), with two of the most studied being the early disk accretion (EDA) and the fast rotating massive star and/or interacting binaries (FRMS/IBs) models. The EDA scenario (e.g. Bastian et al. 2013b) requires low mass stars to

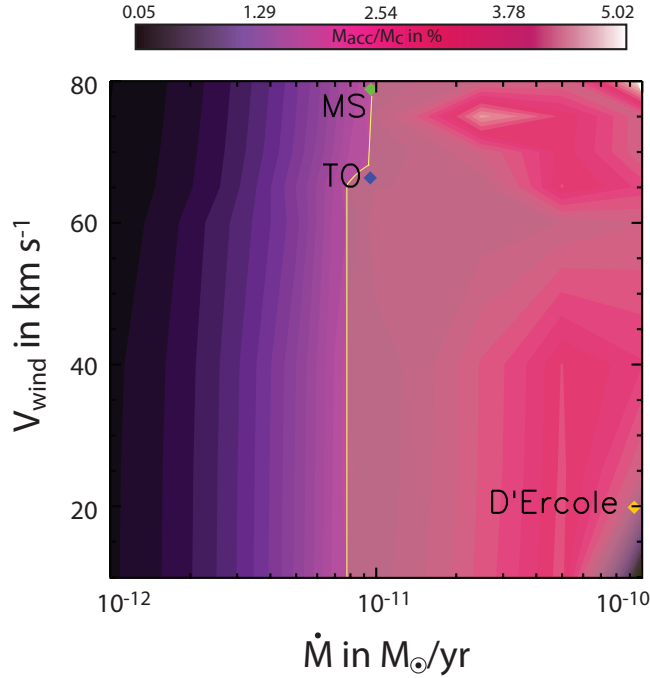


Figure 14. Mass accumulated for a potential with $M_c = 10^7 M_\odot$ and $\sigma_v = 35 \text{ km s}^{-1}$ at 300 Myrs for different \dot{M} and v_w combinations. The shaded region to the right of the yellow line illustrates the parameter space in which star formation is triggered at 300 Myrs. The colored diamonds denote the parameters which prescribe the mass loss rates and wind velocities from our turn off (blue) and population averaged prescriptions (green), along with the parameters from (D'Ercole et al. 2008) (yellow).

sweep up material pre-processed from rotating massive stars and/or interacting high mass binaries, while the FRMS/IBs scenarios (e.g. de Mink et al. 2009; Krause et al. 2013) assumes a second generation of stars forms from the ejecta of rapidly rotating and/or dynamically stripped massive stars within the first 20 – 40 Myrs of a cluster's life. While only a small amount of material is expected to be retained by stellar winds during the time span in which these two scenarios operate (0.5 – 2% between ~ 10 – 50 Myrs in Figures 9 – 11), it is possible that it might have a mitigating effect on these processes. The EDA model requires the pre-main sequence disks to survive for ~ 10 – 20 Myrs. Along with other disk-damaging effects (Scally & Clarke 2001; de Juan Ovelar et al. 2012), the existence of the hot, thermalized stellar wind intercluster medium could aid in the destruction of these pre-main sequence disks from ram pressure stripping during as the star moves through the YMC. Inclusion of hot stellar wind material during the first few tens of Myrs of a cluster's life also poses problems for the FRMS/IBs scenario. If this small amount of stellar wind material efficiently thermalizes with the ejecta of FRMS or IBs, the additional heat might be able to prevent a second generation of star formation. Additionally, the combination of efficient mixing between stellar ejecta at early times could also lead to dispersions in Iron, which are not seen in all but a few clusters (e.g. Villanova et al. 2007).

Other methods of generating a subpopulation of stars with enhanced light element abundances during the early phases of cluster evolution ($\lesssim 500$ Myrs) which either rely on pollution sources that are highly centralized to the core of the proto-GC (Very Massive Stars, Denissenkov & Hartwick 2014; Extended Central Star Formation, Prantzos & Charbonnel 2006; Elmegreen 2017; Wünsch et al. 2017), a top heavy IMF (Charbonnel et al. 2014), more complex gas dynamics during initial phases of star formation (Inhomogeneous Pre-enriched Gas, Marcolini et al. 2009; Turbulent Elemental Sepa-

ration, Hopkins 2014), or the reaccretion of remnant gas (Decressin et al. 2007a,b) are not necessarily inconsistent with our models given that they depend on sources of enrichment that do not follow the stellar potential as we have assumed here. However, fast stellar winds would undoubtedly add to the energy budget in such models, decreasing the gas retention potential of all scenarios.

Indeed, the expected retention and expulsion of gas in YMCs as predicted from our stellar wind only models potentially poses problems for all of the popular explanations of globular cluster formation under the assumption that YMCs evolve into IACs and eventually globular clusters. Given our model's agreement with both the current observed gas content in YMCs (section 6.1.1) and observed ongoing star formation (section 6.1.2), it is possible that the assumption that present day YMCs evolve into present day GCs needs to be relaxed. However, we caution that because current abundance models for all scenarios fail to fully reproduce the distribution of observed abundance anomalies (Bastian et al. 2015), the idea of a single formation pathway and any effects our stellar wind models may have on its success will likely need to be reevaluated as these scenarios evolve.

6.2 Prospects for the Detection of Gas and Star Formation in Intermediate Age Clusters: Age ~ 1 -4 Gyrs

Our models predict the existence of large gas reservoirs during the time period of 1-4 Gyrs in all clusters with $\sigma_v \gtrsim 25 \text{ km s}^{-1}$ and $M \gtrsim 10^6 M_\odot$. In addition, if the main sequence winds thermalize inefficiently with the winds from the turn off stars (Figure 9) or the gas retention in the cluster "has memory" (Figure 11), a small amount of star formation is predicted to be triggered during this time span - approximately $\lesssim 10\%$ of the cluster mass may be available for a second generation of star formation. Assuming the generous

rate of 10% star formation efficiency, this implies only $\sim 1\%$ of the cluster's mass forms stars once the cluster is older than ~ 1 -3 Gyrs. To observe such a small rate of star formation at high precision, we are limited in observations to within the Local Group (~ 1 -2 Mpc) as photometrically derived SFHs in general to agree with CMD derived ones at a level of a few percent, a level which is far higher than the $\lesssim 1\%$ one would need to resolve (Ruiz-Lara et al. 2015). In one of the largest searches for star formation locally in the Magellanic Clouds, no ongoing star formation has been observed in star clusters with ages up to ~ 1 Gyr (Bastian et al. 2013b). For observations of older clusters matters are further complicated as to accurately age data clusters photometrically in the range of 1-4 Gyrs both optical and NIR are necessary to break the strong age-metallicity degeneracy between these and the much older ~ 13 Gyr old clusters (Trancho et al. 2014), making such observations more expensive for clusters older than ~ 1 Gyr.

Merging galaxies provide another possible avenue to observe ongoing star formation and gas retention in massive clusters, albeit at lower precision than in the Local Group, as these systems typically generate a multitude of star cluster formation with ages approximately the age of the merger itself (Whitmore et al. 2007). However observations of one of the most studied mergers, the Antennae galaxies, occurring ~ 500 Myrs ago, shows that while upper limits on gas content show intercluster gas at the level of $\lesssim 9\%$ (Cabrera-Ziri et al. 2015), there are large gas reservoirs surrounding the clusters (Zhu et al. 2003) - hardly the clusters in isolation studied here - making a strict comparison between our prescription and those in intermediate age merging systems less straight forward. Furthermore, external gas reservoirs could either aid in the retention of intercluster gas or help with its expulsion. If the clusters move through hot and/or dense gas ram pressure stripping may be effective at removing material over a few sound crossing times across the cluster (Frank & Gisler 1976; Naiman et al. 2009; de Silva et al. 2009; Martell & Smith 2009; Pancino et al. 2010a; Naiman et al. 2011; Priestley et al. 2011). If, however, they move slowly enough relative to the sound speed of the gas the large reservoir of external material may aid in the retention of gas within the clusters' centers (Pflamm-Altenburg & Kroupa 2009; Naiman et al. 2011; Priestley et al. 2011).

More locally, the effects of gas retention on observations of SMC and LMC star clusters has focused predominately on the YMC population (Bastian & Strader 2014; Longmore 2015). While there are IACs in the LMC and SMC with large extinctions there is not an overall trend with age (Perren et al. 2017) as would be suggested by the work presented here. However, we caution here that once again LMC and SMC clusters are not necessarily the isolated systems discussed in this work.

Finally, if IACs are believed to evolve into GCs, the amounts of gas retained from stars during the 1-4 Gyr time span would possibly lead to subsequent populations of stars with enhanced C+N+O, which is not currently observed in the enhanced population of stars in galactic GCs (Decressin et al. 2009).

While observations of star formation and gas retention in IACs are far from complete, the observed lack of star formation and gas retention implies that there is efficient thermalization between main sequence and evolved stellar winds as depicted in Figure 10 or an additional source of heat in these systems. Additionally, other mechanisms beyond ram pressure stripping and stellar wind feedback may be responsible for clearing the gas. In lower mass and less dense clusters, radiation from white dwarfs may result in the ionization of the gas at ages $\gtrsim 1$ Gyr (McDonald & Zijlstra 2015), and classical novae may be able to drive gas out in the lower mass clusters (Moore & Bildsten 2011). Furthermore, in both low and high mass clusters,

the accretion onto stellar-mass black holes could aid in removing this build up of mass in the system (Leigh et al. 2013).

Both further observations of star formation and gas content in IACs and more physically realistic simulations are needed before a more robust comparison between the stellar wind retention models presented here and the observed properties of IACs can be made.

6.3 Current Gas Content in Globular Clusters: Age $\gtrsim 7$ Gyrs

As there is little to no ongoing star formation predicted in our models and observed in galactic GCs or old SMC and LMC clusters (e.g. Martocchia et al. 2018), we here focus solely on the current gas content of globular clusters.

Given that the typical time between gas stripping Galactic GCs' disk passages, 0.1 Gyrs (Odenkirchen et al. 1997), is long enough for significant slow RGB wind material to be injected into GCs (Tayler & Wood 1975), if this wind material is effectively retained within the cluster we expect to see approximately 10 - $100 M_{\odot}$ of gas within Galactic GCs. However, the majority of Galactic GCs show little or no evidence for gas of 10 - $100 M_{\odot}$ within their interiors, as measured either in neutral hydrogen (Heiles & Henry 1966; Robinson 1967; Kerr & Knapp 1972; Knapp et al. 1973; Bowers et al. 1979; Birkinshaw et al. 1983; Lynch et al. 1989; Smith et al. 1990; van Loon et al. 2006, 2009), CO (Troland et al. 1978; Smith et al. 1995; Leon & Combes 1996), OH and H₂O maser emission (Knapp & Kerr 1973; Kerr et al. 1976; Frail & Beasley 1994; Cohen & Malkan 1979; Dickey & Malkan 1980; van Loon et al. 2006), or dust (Lynch & Rossano 1990; Knapp et al. 1995; Origlia et al. 1996; Hopwood et al. 1998, 1999; Evans et al. 2003; Boyer et al. 2006; Barmby et al. 2009). The most stringent constraints come from a combination of radio dispersion measurements of millisecond pulsars in 47 Tucanae (Camilo et al. 2000) showing $n_e = 0.067 \pm 0.015 \text{ cm}^{-3}$ and neutral hydrogen measurements indicating $M_{\text{HI}} \lesssim 3.7 M_{\odot}$, which when taken together indicate a dearth of gas within 47 Tucanae. In addition, as mentioned in previously in section 6.2, while there are enhancements in extinction in SMC and LMC clusters, it is not a highly ubiquitous feature of the old clusters in these systems (Perren et al. 2017).

In Figures 9 - 11 we find little expected gas retention in all but the most compact star clusters ($\sigma_v \lesssim 40$ – 45 km s^{-1}) at a population age of 10 Gyrs, but caution any gas retention is likely to decrease for less massive clusters ($M_c < 10^7 M_{\odot}$) as indicated in the right hand panel of Figure 9. For $\sigma_v \lesssim 23 \text{ km s}^{-1}$ we find negligible mass retention across all mass loss prescriptions and cluster masses ($M_{\text{acc}}/M_c \sim 0\%$). Thus, our results are in excellent agreement with both observations and a previous analytically derived limit of $\sigma_v \lesssim 22 \text{ km s}^{-1}$ by Smith (1999) who also account for the effects of main sequence stellar wind heating on the intercluster gas.

7 SUMMARY AND CONCLUSIONS

We have presented a grid of spherically symmetric simulations of gas retention and expulsion due to stellar winds within star clusters. While previous work has estimated the ability of star clusters to retain stellar winds (D'Ercole et al. 2008, 2010; Vesperini et al. 2010; Conroy & Spergel 2011; Conroy et al. 2011), calculations have so far been undertaken over a smaller range of cluster properties and stellar ages, typically with lower stellar wind velocities than those argued for in this work. Motivated by this, we have calculated gas retention in star clusters of various ages, stellar mass and compactness. Additionally, we include a discussion of the choice of

the kinetic energy injection proxy, taken here as the wind velocity, v_w , and its relation to the observed distribution of outflow velocities observed in field and globular cluster AGB and RGB stars.

Our main conclusions are the following:

- We conclude that in compact star clusters a choice of $v_w = v_{\text{esc}}$ best reproduces both the observations of stellar winds and the assumed level of mixing between stellar wind and the intercluster medium.
- Given our assumptions about the mass loss rates and wind velocities emanating from stars residing in clusters, we find the optimum time for gas retention is approximately 1-2 Gyrs. However, depending on how efficiently the slow winds from AGB/RGB stars mix with the fast winds from the numerous main sequence cluster members, and how effectively gas is cleared after each episode of star formation within the cluster, we find star formation may not be triggered within this optimum time span as the gas may be too hot.
- We find significant gas retention can occur when cluster velocity dispersions are high, $\sigma_v \gtrsim 25 \text{ km s}^{-1}$, but the amount of gas retained drops as the velocity dispersion grows due to the efficient funneling of gas to the central regions of the cluster and subsequent triggering of star formation for very compact clusters.
- We compare our results with observations of young massive clusters (YMCs), intermediate age clusters (IACs) and globular clusters (GCs). We find our models generally agree with observations. We predict little gas retention and star formation in YMCs and GCs. Our models predict higher levels of gas retention in IACs ($\approx 10\%$ of the stellar mass). However, we caution that both the lack of observations of isolated IAC systems and the lack of inclusion of all the sources of thermal and kinetic energy in star clusters in this age range makes any conclusions drawn from our models preliminary.
- Finally, we discuss the implications of our models on the assumed evolutionary sequence of YMC → IAC → GC resulting in observations of multiple sub-populations with different levels of light element enhancement in present-day GCs. The majority of proposed origins for these sub-populations rely on some amount of gas retention in the age range few-100s of Myrs. However, we find hot stellar winds are effective at driving material from the cluster during this time frame for all but the most massive and compact clusters. This result is problematic for the AGB wind retention scenario (D'Ercole et al. 2008, 2010; Conroy et al. 2011; Conroy & Spergel 2011) invoked to explain the abundance anomalies observed in present day Galactic globular clusters, but if hot stellar winds can effectively thermalize with the intercluster medium during this time, our models pose problems for gas retention in the early disk accretion (Bastian et al. 2013b) and fast rotating massive stars (Krause et al. 2013) scenarios as well.

In this work, we have also tried to minimize the effect of external mass inflow by considering star clusters in isolation. This is certainly not the case for clusters moving through cold, dense environments, as they can potentially amass a significant amount of gas from their surroundings (Naiman et al. 2009, 2011), or clusters moving quickly through hot halo gas or the galactic disk (Priestley et al. 2011). If the star clusters reside within cold gas, stellar winds and exterior inflows

in such clusters could combine to create even larger central density enhancements (Naiman et al. 2009; Pflamm-Altenburg & Kroupa 2009; Naiman et al. 2011; Conroy et al. 2011). Additionally, one dimensional spherically symmetric models cannot accurately model all multi-dimensional phenomena. For example, these simulations are not able to follow the effects of cool fragments which may exist in otherwise hot gas, thereby overestimating the effects of hot gas expelling material from the cluster (Krause et al. 2012). A self consistent treatment of both interior and exterior gas accumulation in multi-dimensional simulations, which includes the effects of compact object accretion, tidal stripping, photoionization, and pulsar heating will be presented elsewhere.

ACKNOWLEDGEMENTS

We thank Mark Krumholz, Charlie Conroy, David Pooley, Rebecca Bernstein, Chung-Pei Ma and Morgan Macleod for useful discussions, and we thank the referee for their helpful comments. The software used in this work was in part developed by the DOE-supported ASCI/Alliance Center for Astrophysical Thermonuclear Flashes at the University of Chicago. Computations were performed on the Pleiades/Hyades UCSC computer cluster. This work is supported by NSF: AST-0847563, NASA: NNX08AL41G, NSF AARF award AST-1402480, and The David and Lucile Packard Foundation.

This paper has been typeset from a $\text{\TeX}/\text{\LaTeX}$ file prepared by the author.

REFERENCES

- Abbott D. C., 1978, *ApJ*, **225**, 893
 Badalyan O. G., Livshits M. A., 1992, *Azh*, **69**, 138
 Barmby P., Boyer M. L., Woodward C. E., Gehrz R. D., van Loon J. T., Fazio G. G., Marengo M., Polomski E., 2009, *AJ*, **137**, 207
 Bastian N., Lardo C., 2017, preprint, ([arXiv:1712.01286](https://arxiv.org/abs/1712.01286))
 Bastian N., Strader J., 2014, *MNRAS*, **443**, 3594
 Bastian N., Lamers H. J. G. L. M., de Mink S. E., Longmore S. N., Goodwin S. P., Gieles M., 2013a, *MNRAS*, **436**, 2398
 Bastian N., Cabrera-Ziri I., Davies B., Larsen S. S., 2013b, *MNRAS*, **436**, 2852
 Bastian N., Hollyhead K., Cabrera-Ziri I., 2014, *MNRAS*, **445**, 378
 Bastian N., Cabrera-Ziri I., Salaris M., 2015, *MNRAS*, **449**, 3333
 Bastian N., et al., 2016, *MNRAS*,
 Beasley M. A., Brodie J. P., Strader J., Forbes D. A., Proctor R. N., Barmby P., Huchra J. P., 2005, *AJ*, **129**, 1412
 Bekki K., 2011, *MNRAS*, **412**, 2241
 Bekki K., Campbell S. W., Lattanzio J. C., Norris J. E., 2007, *MNRAS*, **377**, 335
 Birkinshaw M., Ho P. T. P., Baud B., 1983, *A&A*, **125**, 271
 Bloecker T., 1995a, *A&A*, **297**, 727
 Bloecker T., 1995b, *A&A*, **297**, 727
 Bondi H., Hoyle F., 1944, *MNRAS*, **104**, 273
 Bowers P. F., Kerr F. J., Knapp G. R., Gallagher J. S., Hunter D. A., 1979, *ApJ*, **233**, 553
 Boyer M. L., Woodward C. E., van Loon J. T., Gordon K. D., Evans A., Gehrz R. D., Helton L. A., Polomski E. F., 2006, *AJ*, **132**, 1415
 Briley M. M., Cohen J. G., Stetson P. B., 2002, *ApJ*, **579**, L17
 Brüns R. C., Kroupa P., Fellhauer M., 2009, *ApJ*, **702**, 1268
 Cabrera-Ziri I., Bastian N., Davies B., Magris G., Bruzual G., Schweizer F., 2014, *MNRAS*, **441**, 2754
 Cabrera-Ziri I., et al., 2015, *MNRAS*, **448**, 2224
 Cabrera-Ziri I., et al., 2016, *MNRAS*, **457**, 809
 Caldwell N., Schiavon R., Morrison H., Rose J. A., Harding P., 2011, *AJ*, **141**, 61

- Calar F., Few C. G., Romano D., D'Ercole A., 2015, [ApJ](#), **814**, L14
 Camilo F., Lorimer D. R., Freire P., Lyne A. G., Manchester R. N., 2000, [ApJ](#), **535**, 975
 Cannon R. D., Croke B. F. W., Bell R. A., Hesser J. E., Stathakis R. A., 1998, [MNRAS](#), **298**, 601
 Carretta E., Bragaglia A., Gratton R. G., Leone F., Recio-Blanco A., Lucatello S., 2006, [A&A](#), **450**, 523
 Carretta E., et al., 2009a, [A&A](#), **505**, 117
 Carretta E., Bragaglia A., Gratton R., Lucatello S., 2009b, [A&A](#), **505**, 139
 Carretta E., Bragaglia A., Gratton R., D'Orazi V., Lucatello S., 2009c, [A&A](#), **508**, 695
 Carretta E., Bragaglia A., Gratton R., Lucatello S., Bellazzini M., D'Orazi V., 2010a, [ApJ](#), **712**, L21
 Carretta E., et al., 2010b, [ApJ](#), **714**, L7
 Cassisi S., Salaris M., 2014, [A&A](#), **563**, A10
 Charbonnel C., Krause M., Decressin T., Prantzos N., Meynet G., 2013, *Mem. Soc. Astron. Italiana*, **84**, 158
 Charbonnel C., Chantereau W., Krause M., Primas F., Wang Y., 2014, [A&A](#), **569**, L6
 Choi E., Yi S. K., 2008, [MNRAS](#), **386**, 1332
 Cohen O., 2011, [MNRAS](#), **417**, 2592
 Cohen N. L., Malkan M. A., 1979, [AJ](#), **84**, 74
 Cohen J. G., Briley M. M., Stetson P. B., 2002, [AJ](#), **123**, 2525
 Cohen J. G., Briley M. M., Stetson P. B., 2005, [AJ](#), **130**, 1177
 Conroy C., 2012, [ApJ](#), **758**, 21
 Conroy C., Spergel D. N., 2011, [ApJ](#), **726**, 36
 Conroy C., Loeb A., Spergel D. N., 2011, [ApJ](#), **741**, 72
 Cranmer S. R., Saar S. H., 2011, [ApJ](#), **741**, 54
 D'Antona F., Caloi V., 2004, [ApJ](#), **611**, 871
 D'Ercole A., Vesperini E., D'Antona F., McMillan S. L. W., Recchi S., 2008, [MNRAS](#), **391**, 825
 D'Ercole A., D'Antona F., Ventura P., Vesperini E., McMillan S. L. W., 2010, [MNRAS](#), **407**, 854
 D'Ercole A., D'Antona F., Vesperini E., 2011, [MNRAS](#), **415**, 1304
 Dalgarno A., McCray R. A., 1972, [ARA&A](#), **10**, 375
 Debes J. H., 2006, [ApJ](#), **652**, 636
 Decressin T., Meynet G., Charbonnel C., Prantzos N., Ekström S., 2007a, [A&A](#), **464**, 1029
 Decressin T., Charbonnel C., Meynet G., 2007b, [A&A](#), **475**, 859
 Decressin T., Charbonnel C., Siess L., Palacios A., Meynet G., Georgy C., 2009, [A&A](#), **505**, 727
 Demircan O., Kahraman G., 1991, [Ap&SS](#), **181**, 313
 Denissenkov P. A., Hartwick F. D. A., 2014, [MNRAS](#), **437**, L21
 Dickey J. M., Malkan M. A., 1980, [AJ](#), **85**, 145
 Doherty C. L., Gil-Pons P., Lau H. H. B., Lattanzio J. C., Siess L., 2014a, [MNRAS](#), **437**, 195
 Doherty C. L., Gil-Pons P., Lau H. H. B., Lattanzio J. C., Siess L., Campbell S. W., 2014b, [MNRAS](#), **441**, 582
 Dupree A. K., Reimers D., 1987, in Kondo Y., ed., *Astrophysics and Space Science Library Vol. 129, Exploring the Universe with the IUE Satellite.* pp 321–353, doi:10.1007/978-94-009-3753-6_17
 Dupree A. K., Whitney B. A., Avrett E. H., 1992a, in Giampapa M. S., Bookbinder J. A., eds, *Astronomical Society of the Pacific Conference Series Vol. 26, Cool Stars, Stellar Systems, and the Sun.* p. 525
 Dupree A. K., Sasselov D. D., Lester J. B., 1992b, [ApJ](#), **387**, L85
 Dupree A. K., Smith G. H., Strader J., 2009, [AJ](#), **138**, 1485
 Elmegreen B. G., 2017, [ApJ](#), **836**, 80
 Evans A., Stickel M., van Loon J. T., Eyres S. P. S., Hopwood M. E. L., Penny A. J., 2003, [A&A](#), **408**, L9
 Evans C. J., Lennon D. J., Trundle C., Heap S. R., Lindler D. J., 2004, [ApJ](#), **607**, 451
 Faulkner D. J., Freeman K. C., 1977, [ApJ](#), **211**, 77
 Fenner Y., Campbell S., Karakas A. I., Lattanzio J. C., Gibson B. K., 2004, [MNRAS](#), **353**, 789
 Ferraro F. R., et al., 2009, [Nature](#), **462**, 483
 Frail D. A., Beasley A. J., 1994, [A&A](#), **290**, 796
 Frank J., Gisler G., 1976, [MNRAS](#), **176**, 533
 Fryxell B., et al., 2000, [ApJS](#), **131**, 273
 Gerssen J., van der Marel R. P., Gebhardt K., Guhathakurta P., Peterson R. C., Pryor C., 2002, [AJ](#), **124**, 3270
 Gnat O., Sternberg A., 2007, [ApJS](#), **168**, 213
 Goudfroij P., et al., 2014, [ApJ](#), **797**, 35
 Gratton R. G., et al., 2001, [A&A](#), **369**, 87
 Gratton R., Sneden C., Carretta E., 2004, [ARA&A](#), **42**, 385
 Harris W. E., 1996, [AJ](#), **112**, 1487
 Heiles C., Henry R. C., 1966, [ApJ](#), **146**, 953
 Hénault-Brunet V., Gieles M., Agertz O., Read J. I., 2015, [MNRAS](#), **450**, 1164
 Hollyhead K., Bastian N., Adamo A., Silva-Villa E., Dale J., Ryon J. E., Gazak Z., 2015, [MNRAS](#), **449**, 1106
 Hopkins P. F., 2014, [ApJ](#), **797**, 59
 Hopwood M. E. L., Evans A., Penny A., Eyres S. P. S., 1998, [MNRAS](#), **301**, L30
 Hopwood M. E. L., Eyres S. P. S., Evans A., Penny A., Odenkirchen M., 1999, [A&A](#), **350**, 49
 Hueyotl-Zahuantitla F., Tenorio-Tagle G., Wünsch R., Silich S., Palouš J., 2010, [ApJ](#), **716**, 324
 Ivans I. I., Sneden C., Kraft R. P., Suntzeff N. B., Smith V. V., Langer G. E., Fulbright J. P., 1999, [AJ](#), **118**, 1273
 Kalirai J. S., 2013, *Mem. Soc. Astron. Italiana*, **84**, 58
 Kalirai J. S., et al., 2013, [ApJ](#), **763**, 110
 Karakas A., Lattanzio J. C., 2007, [Publ. Astron. Soc. Australia](#), **24**, 103
 Karakas A. I., Fenner Y., Sills A., Campbell S. W., Lattanzio J. C., 2006, [ApJ](#), **652**, 1240
 Kerr F. J., Knapp G. R., 1972, [AJ](#), **77**, 573
 Kerr F. J., Bowers P. F., Knapp G. R., 1976, in *Bulletin of the American Astronomical Society*. p. 537
 Knapp G. R., Kerr F. J., 1973, [AJ](#), **78**, 458
 Knapp G. R., Rose W. K., Kerr F. J., 1973, [ApJ](#), **186**, 831
 Knapp G. R., Gunn J. E., Connolly A. J., 1995, [ApJ](#), **448**, 195
 Kraft R. P., Sneden C., Langer G. E., Shetrone M. D., 1993, [AJ](#), **106**, 1490
 Krause M., Charbonnel C., Decressin T., Meynet G., Prantzos N., Diehl R., 2012, [A&A](#), **546**, L5
 Krause M., Charbonnel C., Decressin T., Meynet G., Prantzos N., 2013, [A&A](#), **552**, A121
 Kroupa P., 2001, [MNRAS](#), **322**, 231
 Kroupa P., Weidner C., Pfamm-Altenburg J., Thies I., Dabringhausen J., Marks M., Maschberger T., 2013, *The Stellar and Sub-Stellar Initial Mass Function of Simple and Composite Populations.* p. 115, doi:10.1007/978-94-007-5612-0_4
 Kruijssen J. M. D., 2015, [MNRAS](#), **454**, 1658
 Külebi B., Kalirai J., Jordan S., Euchner F., 2013, [A&A](#), **554**, A18
 Lada C. J., Lada E. A., 2003, [ARA&A](#), **41**, 57
 Larsen S. S., et al., 2011, [A&A](#), **532**, A147
 Leigh N. W. C., Böker T., Maccarone T. J., Perets H. B., 2013, [MNRAS](#), **429**, 2997
 Leon S., Combes F., 1996, [A&A](#), **309**, 123
 Li C., de Grijs R., Deng L., Geller A. M., Xin Y., Hu Y., Faucher-Giguère C.-A., 2016, [Nature](#), **529**, 502
 Longmore S. N., 2015, [MNRAS](#), **448**, L62
 Longmore S. N., et al., 2014, *Protostars and Planets VI*, pp 291–314
 Loup C., Forveille T., Omont A., Paul J. F., 1993, [A&AS](#), **99**, 291
 Lynch D. K., Rossano G. S., 1990, [AJ](#), **100**, 719
 Lynch D. K., Bowers P. F., Whiteoak J. B., 1989, [AJ](#), **97**, 1708
 Maeder A., Meynet G., 2006, [A&A](#), **448**, L37
 Marcolini A., Gibson B. K., Karakas A. I., Sánchez-Blázquez P., 2009, [MNRAS](#), **395**, 719
 Marigo P., 2012, in *IAU Symposium.* pp 87–94, doi:10.1017/S1743921312010757
 Marino A. F., Milone A. P., Piotti G., Villanova S., Bedin L. R., Bellini A., Renzini A., 2009, [A&A](#), **505**, 1099
 Martell S. L., Smith G. H., 2009, [PASP](#), **121**, 577
 Martell S. L., Duffau S., Milone A. P., Smith G. H., Briley M. M., Grebel E. K., 2013, *Mem. Soc. Astron. Italiana*, **84**, 42
 Martocchia S., et al., 2018, [MNRAS](#), **473**, 2688
 Mauas P. J. D., Cacciari C., Pasquini L., 2006, [A&A](#), **454**, 609

- McDonald I., Zijlstra A. A., 2015, *MNRAS*, **446**, 2226
 McDonald I., van Loon J. T., 2007, *A&A*, **476**, 1261
 McNamara B. J., Harrison T. E., Baumgardt H., 2004, *ApJ*, **602**, 264
 Mészáros S., Avrett E. H., Dupree A. K., 2009, *AJ*, **138**, 615
 Milone A. P., Marino A. F., D'Antona F., Bedin L. R., Da Costa G. S., Jerjen H., Mackey A. D., 2016, *MNRAS*, **458**, 4368
 Moore K., Bildsten L., 2011, *ApJ*, **728**, 81
 Morin J., et al., 2008, *MNRAS*, **390**, 567
 Mucciarelli A., 2014, *Mem. Soc. Astron. Italiana*, **85**, 276
 Mucciarelli A., Carretta E., Origlia L., Ferraro F. R., 2008, *AJ*, **136**, 375
 Naiman J. P., Ramirez-Ruiz E., Lin D. N. C., 2009, *ApJ*, **705**, L153
 Naiman J. P., Ramirez-Ruiz E., Lin D. N. C., 2011, *ApJ*, **735**, 25
 Nyman L.-A., et al., 1992, *A&AS*, **93**, 121
 Odenkirchen M., Brosche P., Geffert M., Tucholke H.-J., 1997, *New Astron.*, **2**, 477
 Origlia L., Ferraro F. R., Pecci F. F., 1996, *MNRAS*, **280**, 572
 Pancino E., Carrera R., Rossetti E., Gallart C., 2010a, *A&A*, **511**, A56
 Pancino E., Rejkuba M., Zoccali M., Carrera R., 2010b, *A&A*, **524**, A44
 Pasquato M., de Luca A., Raimondo G., Carini R., Moraghan A., Chung C., Brocato E., Lee Y.-W., 2014, *ApJ*, **789**, 28
 Paxton B., Bildsten L., Dotter A., Herwig F., Lesaffre P., Timmes F., 2011, *ApJS*, **192**, 3
 Peacock M. B., Zepf S. E., Finzell T., 2013, *ApJ*, **769**, 126
 Perren G. I., Piatti A. E., Vázquez R. A., 2017, *A&A*, **602**, A89
 Pflamm-Altenburg J., Kroupa P., 2009, *MNRAS*, **397**, 488
 Piatti A. E., Bastian N., 2016, preprint, ([arXiv:1603.06891](https://arxiv.org/abs/1603.06891))
 Piotto G., et al., 2007, *ApJ*, **661**, L53
 Pooley D., Rappaport S., 2006, *ApJ*, **644**, L45
 Pooley D., et al., 2003, *ApJ*, **591**, L131
 Portegies Zwart S. F., McMillan S. L. W., Gieles M., 2010, *ARA&A*, **48**, 431
 Prantzos N., Charbonnel C., 2006, *A&A*, **458**, 135
 Prantzos N., Charbonnel C., Iliadis C., 2007, *A&A*, **470**, 179
 Priestley W., Ruffert M., Salaris M., 2011, *MNRAS*, **411**, 1935
 Quataert E., 2004, *ApJ*, **613**, 322
 Reimers D., 1975, *Memoires of the Societe Royale des Sciences de Liege*, **8**, 369
 Robinson B. J., 1967, *Astrophys. Lett.*, **1**, 21
 Rodríguez-González A., Esquivel A., Raga A. C., Cantó J., 2008, *ApJ*, **684**, 1384
 Rogers H., Pittard J. M., 2013, *MNRAS*, **431**, 1337
 Ruiz-Lara T., et al., 2015, *A&A*, **583**, A60
 Scally A., Clarke C., 2001, *MNRAS*, **325**, 449
 Schaefer D., de Koter A., Schmutz W., Maeder A., 1996, *A&A*, **310**, 837
 Searle S. C., Prinja R. K., Massa D., Ryans R., 2008, *A&A*, **481**, 777
 Smith G. H., 1999, *PASP*, **111**, 980
 Smith G. H., Dupree A. K., 1988, *AJ*, **95**, 1547
 Smith G. H., Wood P. R., Faulkner D. J., Wright A. E., 1990, *ApJ*, **353**, 168
 Smith G. H., Woodsworth A. W., Hesser J. E., 1995, *MNRAS*, **273**, 632
 Smith G. H., Dupree A. K., Strader J., 2004, *PASP*, **116**, 819
 Sneden C., Kraft R. P., Guhathakurta P., Peterson R. C., Fulbright J. P., 2004, *AJ*, **127**, 2162
 Tayler R. J., Wood P. R., 1975, *MNRAS*, **171**, 467
 Tenorio-Tagle G., Bodenheimer P., Lin D. N. C., Noriega-Crespo A., 1986, *MNRAS*, **221**, 635
 Tranco G., Miller B. W., Schweizer F., Burdett D. P., Palamara D., 2014, *ApJ*, **790**, 122
 Troland T. H., Hesser J. E., Heiles C., 1978, *ApJ*, **219**, 873
 Truelove J. K., Klein R. I., McKee C. F., Holliman II J. H., Howell L. H., Greenough J. A., 1997, *ApJ*, **489**, L179
 Usher C., et al., 2015, *MNRAS*, **446**, 369
 Vassiliadis E., Wood P. R., 1993, *ApJ*, **413**, 641
 Ventura P., D'Antona F., 2008a, *MNRAS*, **385**, 2034
 Ventura P., D'Antona F., 2008b, *A&A*, **479**, 805
 Ventura P., D'Antona F., Mazzitelli I., 2000, *A&A*, **363**, 605
 Ventura P., D'Antona F., Mazzitelli I., Gratton R., 2001, *ApJ*, **550**, L65
 Vesperini E., McMillan S. L. W., D'Antona F., D'Ecole A., 2010, *ApJ*, **718**, L112
 Villanova S., et al., 2007, *ApJ*, **663**, 296
 Villaver E., García-Segura G., Manchado A., 2003, *ApJ*, **585**, L49
 Villaver E., Manchado A., García-Segura G., 2012, *ApJ*, **748**, 94
 Waters L. B. F. M., Cote J., Lamers H. J. G. L. M., 1987, *A&A*, **185**, 206
 Whitmore B. C., Chandar R., Fall S. M., 2007, *AJ*, **133**, 1067
 Wilkin F. P., 1996, *ApJ*, **459**, L31
 Wood B. E., Müller H.-R., Zank G. P., Linsky J. L., Redfield S., 2005, *ApJ*, **628**, L143
 Wünsch R., Palouš J., Tenorio-Tagle G., Ehlerová S., 2017, *ApJ*, **835**, 60
 Zhao J. K., Oswalt T. D., Willson L. A., Wang Q., Zhao G., 2012, *ApJ*, **746**, 144
 Zhu M., Seaquist E. R., Kuno N., 2003, *ApJ*, **588**, 243
 de Jager C., Nieuwenhuijzen H., van der Hucht K. A., 1988, *A&AS*, **72**, 259
 de Juan Ovelar M., Kruijsen J. M. D., Bressert E., Testi L., Bastian N., Cánovas H., 2012, *A&A*, **546**, L1
 de Mink S. E., Pols O. R., Langer N., Izzard R. G., 2009, *A&A*, **507**, L1
 de Silva G. M., Gibson B. K., Lattanzio J., Asplund M., 2009, *A&A*, **500**, L25
 van Loon J. T., Stanimirović S., Evans A., Muller E., 2006, *MNRAS*, **365**, 1277
 van Loon J. T., Stanimirović S., Putman M. E., Peek J. E. G., Gibson S. J., Douglas K. A., Korpela E. J., 2009, *MNRAS*, **396**, 1096